Designing a fully-tunable and versatile TKE-l turbulence parameterization for atmospheric models

É. Vignon[1], K. Arjdal[1,2], F. Cheruy[1], M. Coulon-Decorzens[1], C. Dehondt[3], T. Dubos[1], S. Fromang[3], F. Hourdin[1], L. Lange[1], L. Raillard[1], G. Rivière[1], R. Roehrig[4], A. Sima[1], A. Spiga[1], P. Tiengou[1,5]

[1]Laboratoire de Météorologie Dynamique- IPSL, Sorbonne Université/CNRS/ Ecole Normale Supérieure-PSL Université/ Ecole Polytechnique-Institut Polytechnique de Paris, Paris, France
[2]International Water Research Institute (IWRI), CSAES - Mohammed VI Polytechnic University, Benguerir, Morocco
[3]Laboratoire des Sciences du Climat et de l'Environnement, LSCE/IPSL, CEA-CNRS-UVSQ, Université Paris-Saclay, F-91191, Gif-sur-Yvette, France.
[4]CNRM, Université de Toulouse, Météo-France, CNRS, Toulouse, France
[5]Milieux environnementaux, tranferts et interaction dans les hydrosystemes et les sols (Metis)/Sorbonne Université/IPSL/CNRS/ EPHE, Paris, France

Key Points:

- A simple TKE-l turbulent diffusion scheme is developed in a semi-heuristic way for applications in models of the Earth and Mars atmospheres.
- The parameterization is designed to be completely tunable and numerically stable at typical GCM time steps.
- The parameterization is tuned over 1D simulations and is able to capture the Antarctic and Martian stable boundary layers in 3D simulations.

Corresponding author: Étienne Vignon, `etienne.vignon@lmd.ipsl.fr`

Abstract

This study presents the development of a TKE-l parameterization of the diffusion coefficients for the representation of turbulent diffusion in neutral and stable conditions in large-scale atmospheric models. The parameterization has been carefully designed to be completely tunable in the sense that all adjustable parameters have been clearly identified and their number minimized as much as possible to help the calibration and to thoroughly assess the parametric sensitivity. We choose a mixing length formulation that depends on both static stability and wind shear to cover the different regimes of stable boundary layers. We follow a heuristic approach for expressing the stability functions and turbulent Prandtl number in order to guarantee the versatility of the scheme and its applicability for planetary atmospheres composed of an ideal and perfect gas such as that of Earth and Mars. Particular attention has also been paid to the numerical stability at typical time steps used in General Circulation Models. Test, parametric sensitivity assessment and preliminary tuning are performed on single-column idealized simulations of the weakly stable boundary layer. The robustness and versatility of the scheme are also assessed through its implementation in the LMDZ General Circulation Model and the Mars Planetary Climate Model and by running simulations of the Antarctic and Martian nocturnal boundary layers.

Plain Language Summary

In planetary atmospheres, turbulent motions actively contribute to the mixing of quantities such as heat, momentum and chemical species. Such motions are not resolved in coarse-grid atmospheric models and have to be parameterized. The parameterization of turbulent mixing should be based on physical laws and sufficiently sophisticated to realistically represent the full spectrum of motions over the full range of stability encountered in the atmospheres. However, it also necessarily contains a number of closure parameters not always well identified and whose values are determined empirically - thereby questioning the universality of the parameterization and its potential application over the full globe or even to other planets - or adjusted to guarantee the numerical stability of the model. This study presents the design of a turbulent mixing parameterization that can be fully calibrated and applied in planetary atmospheres such as that of Mars. We then calibrate the parameterization on an idealised simulation set-up and test its robustness and performance by running simulations of the Antarctic and Martian atmospheres.

1 Introduction

Turbulence efficiently transports momentum, energy, moisture and matter in the atmosphere, particularly in the planetary boundary layer where it controls sensible and latent heat fluxes as well as the transfer of momentum between the air and the ground surface. It thereby directly affects the diurnal cycle of the near-surface atmospheric quantities and also impacts on the lifetime and structure of synoptic-scale dynamical systems. Turbulent transport is therefore an essential component of the physics of climate models, numerical weather prediction models and more generally of General Circulation Models (GCMs) of planetary atmospheres. As turbulent eddies manifests on scales ranging from a few millimeters to a few tens of kilometers in deep convective systems, modellers develop conceptually separated subgrid parameterizations targeting different types - or different scales - of transport processes. Non-local turbulent transport resulting from large and organised convective cells, being deep or shallow, is often treated with so-called mass flux schemes (e.g., Tiedtke (1989); Emanuel (1991); Hourdin et al. (2002); Golaz et al. (2002)). Local turbulent mixing which results from eddies whose typical size is smaller or similar to the typical grid cell thickness - namely a few tens of meters - is often parameterized with a local K-gradient diffusion scheme. In those schemes, the turbulent flux is parameterized with a Fick's law type down-gradient diffusion formulation that relies on the introduction of a turbulent diffusion coefficient. Such schemes are particularly critical to simulate the stable and neutral

atmospheric boundary layers (Delage, 1997; Cuxart et al., 2006; Sandu et al., 2013), the land-atmosphere coupling as well as the thermal inversion at the top of convective boundary layers.
Several K-gradient diffusion parameterizations have been developed since the pioneering work of Louis (1979) and have been the subject of a substantial body of literature in atmospheric sciences. Among them, the moderate-complexity 1.5 order schemes, or TKE-l schemes, consist in expressing the diffusion coefficients as function of a diagnostic vertical turbulent length-scale, or mixing length, and of a prognostic estimation of the Turbulent Kinetic Energy (TKE) (Mellor & Yamada, 1982; Yamada, 1983).

The closure of the TKE evolution equation and the empirical and/or heuristic formulation of the mixing-length necessarily introduce free parameters in the parameterization, and therefore a certain degree of empiricism in the expression of the diffusion coefficients (Li et al., 2016). Indeed, such parameters do not have, by essence, fixed and universal values. Some of them - and the associated variability range thereof - are determined empirically using field observations, laboratory experiments, Large Eddy Simulations (LES) or Direct Numerical Simulations (DNS) while others are arbitrarily set. In practice, in climate and numerical weather prediction models, the value of some coefficients is often retuned to match large-scale or meteorological targets. For instance as all subgrid mixing processes are not parameterized - such as small scale internal waves or submeso-scale motions - the mixing in stable conditions is often artificially enhanced to prevent unrealistic runaway surface cooling due to surface-atmosphere mechanical decoupling and to maintain sufficient surface drag and Ekman pumping in extratropical cyclones (Holtslag et al., 2013; Sandu et al., 2013). Such empiricism and Earth-oriented tuning can somewhat question the applicability of these turbulent mixing parameterizations in planetary GCMs, even in GCMs of Mars (e.g., Forget et al. (1999); Colaïtis et al. (2013)) where the planetary boundary layer shares similarities with that on Earth (Spiga et al., 2010a).

In addition, arbitrary parameter calibration - sometimes beyond reasonable ranges - is often required to improve the numerical convergence and stability of the parameterization once it is implemented in models with typical physics time steps of a few minutes to a few tens of minutes. Indeed, the numerical implementation of a K-gradient turbulence scheme is prone to spurious oscillations called 'fibrillations' (Kalnay & Kanamitsu, 1988; Girard & Delage, 1990). Such fibrillations are due to *i)* the coupling between momentum and potential temperature via the turbulent diffusion coefficients and *ii)* the discretization of the vertical diffusion in which the nonlinear exchange coefficient is often treated explicitly in time. Even though the TKE budget is often close to a local equilibrium (Lenderink & Holtslag, 2004), the prognostic prediction of the TKE generally makes TKE-l schemes less sensitive to the time discretization and less prone to fibrillation than traditional first-order schemes (Bougeault & Lacarrère, 1989; Bazile et al., 2011) in which the diffusion coefficients are explicit and diagnostic functions of the mean static stability and wind shear (Louis, 1979; Louis et al., 1982; Delage, 1997). This is mostly explained by the fact that the prognostic TKE plays a role of 'reservoir' that damps the sometimes abrupt evolution of the diffusion coefficients with time (Mašek et al., 2022). However, even TKE-based schemes can also be affected by numerical instabilities which can be related to the numerical treatment of the TKE equation itself (Deleersnijder, 1992; Vignon et al., 2018) or to the coupling with other prognostic quantities such as the turbulent potential energy (Mašek et al., 2022). The numerical treatment of the TKE equation and more generally of the turbulent diffusion thereby comes out as a forefront issue in atmospheric modeling. Hence, one has to find a good trade-off between the complexity and sophistication of a turbulent mixing scheme and its practical implementation in large scale atmospheric models avoiding as much as possible unrealistic parameter calibration to guarantee numerical stability and fair model performances.

The sensitivity of the stable boundary layer representation to turbulent diffusion calibration in a large scale atmospheric model was assessed in a game-changing study by Audouin et al. (2021) using a semi-automatic tuning tool based on uncertainty quantification (Couvreux et al., 2021; Hourdin et al., 2021). The authors identified a few key tuning parameters - and their acceptable ranges of values - in the TKE-l turbulent diffusion scheme of the ARPEGE-Climat model and assessed to what extent biases in the simulation of the extremely stable Antarctic boundary layer are explained by structural parameterization deficiencies or tuning choices. However, the boundary layer and surface layer schemes of ARPEGE-Climat contain a large number of tuning parameters, sometimes subtly interdependent, and considering all of them in a tuning exercise may be confusing, thereby challenging.
The present study aims to design a new and simple TKE-l turbulent diffusion scheme for large scale atmospheric models

1. that is sufficiently robust and versatile to be applicable on both Earth and Mars, and potentially on other planetary atmospheres and ;
2. that is built to be completely tuned in the sense that all adjustable parameters are clearly identified and their number minimized to help the calibration - or parameter adjustment - and assess the parametric sensitivity.

The scheme will be referred to as the ATKE scheme - for Adjustable TKE-l scheme - in the paper.

We follow a simple heuristic approach - as in Lenderink and Holtslag (2004) and He et al. (2019) - for expressing the stability functions and turbulent Prandlt number to guarantee the versatility of the scheme and its potential applicability for planetary atmospheres composed of an ideal and perfect gas. A particular attention is also paid to the numerical treatment of the TKE prognostic equation to ensure the numerical stability even in conditions of strong wind shear or strong stratification. It is worth emphasizing that the 'local' nature of the scheme makes it mostly adapted for neutral and stably stratified conditions, hence the particular focus on stable boundary layers in the paper. The scheme is tested and tuned - using the same Uncertainty Quantification approach as in Audouin et al. (2021) and Hourdin et al. (2021) - on idealized single column simulations of the stable boundary layer. The parameterization is then implemented and tested in the Earth LMDZ GCM (Hourdin et al., 2020; Cheruy et al., 2020) and the Mars Planetary Climate model (Forget et al., 1999) to verify its robustness and assess its performances when challenging the stable Antarctic and Martian nocturnal boundary layers.

2 Parameterization development

This section presents the derivation of the ATKE scheme, starting briefly and purposely with some generalities to clearly set the parameterization in the framework of turbulent diffusion in GCMs of planetary atmospheres.

2.1 General framework

The conservation law for an extensive quantity c - being for example the potential temperature, wind components or concentration in chemical species - in a compressible atmosphere reads:

$$\frac{\partial \rho c}{\partial t} + \vec{\nabla}(\rho \vec{u} c) = P_c \tag{1}$$

With, in Cartesian coordinates (x, y, z), $\vec{u} = u\vec{i} + v\vec{j} + w\vec{k}$ the wind vector, ρ the air density and P_c the net source/loss term. We note the statistical (ensemble) average with an overline and introduce the air weighting average operator $\sim$ such that

$$\tilde{c} = \frac{\overline{\rho c}}{\overline{\rho}} \tag{2}$$

Note that $\tilde{c}$ is an extensive variable per mass unit. We decompose c into a mean state and a fluctuation such that $c = \tilde{c} + c'$. We then apply the statistical average operator (overline) on Eq. 1 that now reads:

$$\underbrace{\frac{\partial \overline{\rho}\tilde{c}}{\partial t} + \vec{\nabla}(\overline{\rho}\tilde{c}\tilde{\vec{u}})}_{(1)} = \underbrace{-\vec{\nabla}(\overline{\rho \vec{u}' c'}) + \overline{P_c}}_{(2)} \tag{3}$$

In large-scale atmospheric models the scale separation is imposed by the size of the grid cells which determines the resolved and unresolved components. In this framework, the term (1) in Eq.3 is handled by the dynamical core while the term (2) is the essence of the physical subgrid parameterizations. Further assuming that the subgrid horizontal variations of c are dominated by vertical variations, it follows that $\vec{\nabla}(\overline{\rho \vec{u}' c'}) \approx \partial_z(\overline{\rho w' c'})$. A local turbulent mixing parameterization aims at calculating a tendency on the mean state variable $\tilde{c}$ due to the vertical turbulent diffusion as follows:

$$\left.\frac{\partial \tilde{c}}{\partial t}\right|_{diffusion} = -\frac{1}{\overline{\rho}} \frac{\partial \overline{\rho w' c'}}{\partial z} \tag{4}$$

For better readability and conciseness, we leave the $\sim$ notation out for mean state quantities and note $\rho = \overline{\rho}$ in the following.

For local and mostly shear driven turbulent eddies, the mixing of any conservative quantity during turbulent mixing - such as the common Betts (1973)' variables - can be represented as a diffusive process (e.g. Louis (1979)). Turbulent fluxes can then be expressed with a down-gradient form: $\overline{\rho w' c'} = -\rho K_c \partial_z c$, K_c being a diffusion coefficient. Eq. 4 hence reads:

$$\left.\frac{\partial c}{\partial t}\right|_{diffusion} = \frac{1}{\rho} \frac{\partial}{\partial z} \left(\rho K_c \frac{\partial}{\partial z} c \right) \tag{5}$$

Once the K_c coefficient has been calculated at vertical model layer interfaces, such an equation can be numerically solved with an implicit approach through the inversion of a tri-diagonal matrix.

We now focus on the closure of the K_c coefficient which is the main scope of the present study. We follow here an approach historically proposed by Mellor and Yamada (1974); Yamada (1975) that is, a 1.5 order closure or TKE-l scheme. In this framework, K_c coefficients are expressed as the product of a vertical turbulent length scale or mixing length l with a turbulent vertical velocity scale taken proportional to the square root of the TKE $e = \frac{1}{2}(\overline{u'^2} + \overline{v'^2} + \overline{w'^2})$. The latter is multiplied by a stability function S_c that accounts for the fact that the turbulence anisotropy - thus the contribution of TKE to vertical turbulent mixing - varies with the local stability of the atmosphere characterized by the gradient Richardson number Ri. The diffusion coefficient K_c is then expressed as (Yamada, 1983; Zilitinkevich et al., 2007):

$$K_c = l S_c(Ri)\sqrt{e} \tag{6}$$

In the following sections, we describe the estimation of the three different terms of K_c, namely e, S_c and l. As we want our turbulent scheme to be applicable on Earth and Mars (and potentially other planetary environments), we have to ensure that their expressions are as planet-independent as possible.

2.2 TKE prognostic equation

2.2.1 Parameterization of the source and loss terms

Assuming the horizontal homogeneity of the subgrid-scale statistics, the TKE obeys the following evolution equation (Stull, 1990):

$$\frac{\partial e}{\partial t} = \underbrace{-\overline{u'w'}\frac{\partial u}{\partial z} - \overline{v'w'}\frac{\partial v}{\partial z}}_{\mathcal{W}} + \underbrace{\overline{b'w'}}_{\mathcal{B}} \underbrace{-\frac{1}{\rho}\frac{\partial}{\partial z}(\overline{\rho w'e} + \overline{w'p'})}_{\mathcal{T}} \underbrace{-\epsilon}_{\mathcal{D}} \tag{7}$$

$\mathcal{W}$ is the wind shear production term that can be expressed with the down-gradient expression of fluxes with a diffusion coefficient for momentum hereafter denoted as K_m:

$$-\overline{u'w'}\frac{\partial u}{\partial z} - \overline{v'w'}\frac{\partial v}{\partial z} = K_m S^2 = l S_m \sqrt{e} S^2 \tag{8}$$

with $S^2 = (\partial_z u)^2 + (\partial_z v)^2$ the wind shear and S_m the stability function for momentum. $\mathcal{B}$ is the buoyancy b production/consumption term. For a dry air under the ideal gas assumption, one can write:

$$\overline{b'w'} = \frac{-g}{\rho} \left.\frac{\partial \rho}{\partial \theta}\right|_p \overline{w'\theta'} = \frac{g}{\theta}\overline{w'\theta'} = -K_h \frac{g}{\theta}\frac{\partial \theta}{\partial z} = -K_h N^2 = -l S_h \sqrt{e} N^2 \tag{9}$$

where g is the gravity acceleration of the planet, θ the potential temperature, N the Brünt-Väisälä pulsation, K_h the diffusion coefficient for heat and S_h the stability function for heat. In the case of an atmosphere containing water vapor or chemical species ξ, buoyancy reads $\overline{b'w'} = \frac{-g}{\rho}(\left.\frac{\partial \rho}{\partial \theta}\right|_{p,\xi} \overline{w'\theta'} + \left.\frac{\partial \rho}{\partial \xi}\right|_{p,\theta} \overline{w'\xi'})$. For water vapor - in absence of phase change - or for non-reactive chemical species, one can define a virtual temperature T_v (and a subsequent virtual potential temperature θ_v) corresponding to the temperature that dry air would have if its pressure and density were equal to those of a given sample of the mixture of gas. In this case:

$$\overline{b'w'} \simeq \frac{g}{\theta_v}\overline{w'\theta_v'} = -\frac{g}{\theta_v} K_h \frac{\partial \theta_v}{\partial z} \tag{10}$$

It is worth noting here that the expression of the buoyancy term (or Brünt-Väisälä pulsation) is gravity-dependent thus planet-dependent. For simplicity and consistency with previous literature on turbulent mixing schemes, we keep the formalism with explicit gravity in the following. However, a more universal derivation of the scheme can be achieved with a gravity-invariant formulation of the TKE and turbulent diffusion equations. Such a formulation is proposed in Appendix A.

$\mathcal{D}$ is the viscous TKE dissipation term that can be expressed following Kolmogorov (1941):

$$\epsilon = \frac{e^{3/2}}{l_\epsilon} \tag{11}$$

with l_ϵ the dissipation length-scale characterizing the size of the most dissipative and energy-containing eddies. Following for instance Yamada (1983) and Bougeault and Lacarrère (1989), we assume that l_ϵ scales with l such that $l_\epsilon = c_\epsilon l$, c_ϵ being a scalar. Its value roughly ranges between 1.2 and 10.0 (Yamada, 1983; Audouin et al., 2021; He et al., 2019) since dissipation length scale - characterizing the dissipation of turbulence as a whole - might be larger than vertical mixing length in stable conditions due to the fact that kinetic energy can dissipate through wavy motion with little transfer to the smaller turbulent scales (Cuxart et al., 2006).

The vertical turbulent flux of TKE and the pressure term gathered in $\mathcal{T}$ redistribute TKE through the depth of the atmospheric column. Hence, those two terms are commonly grouped together and expressed as a TKE turbulent diffusion term:

$$-\frac{1}{\rho}\frac{\partial}{\partial z}(\overline{\rho w'e}+\overline{w'p'}) = \frac{1}{\rho}\frac{\partial}{\partial z}(\rho K_e\frac{\partial e}{\partial z}) \tag{12}$$

K_e being taken proportional to K_m (Yamada, 1983; Bougeault & Lacarrère, 1989; Lenderink & Holtslag, 2004): $K_e = c_e K_m$. c_e is a constant whose value is generally around 1 - 2 and that we will arbitrarily allow to vary between 1 and 5 (Bougeault & Lacarrère, 1989; Lenderink & Holtslag, 2004; Baas et al., 2018). The lower boundary condition of e that is, the surface value of the TKE e_s, is estimated by assuming stationary near-neutral conditions in the surface layer. On such a condition (Baas et al., 2018; Lenderink & Holtslag, 2004):

$$e_s = c_s u_*^2 \tag{13}$$

with c_s a constant and u_* the surface friction velocity calculated from the surface drag coefficient for momentum and the wind speed at the first model level. A proper scaling of the TKE-l parameterization with the Monin-Obukhov similarity in the surface layer requires (He et al., 2019):

$$c_s = c_\epsilon^{2/3} \tag{14}$$

2.2.2 Numerical treatment

Once the different TKE source and loss terms have been expressed, Eq. 7 has to be integrated in time. The numerical treatment of Eq. 7 is critical as the solution must be stable and converge at typical physical time steps used in atmospheric GCMs namely, of the order of $\approx$ 15 min. Several methods have been proposed in the literature, particularly regarding the treatment of the dissipation term with different degrees of implicitation (Bazile et al., 2011).

Here, we propose a 2-step resolution method which allows for an exact treatment of the dissipation term - under some assumptions - while the transport term is calculated separately.

Step 1 We calculate the TKE tendency due to the shear, buoyancy and dissipation terms. Noting $q = \sqrt{2e}$, one can rewrite Eq. 7 with no transport term as:

$$\frac{\partial q}{\partial t} = \frac{lS_m}{\sqrt{2}}S^2\left(1-\frac{Ri}{Pr}\right) - \frac{q^2}{2^{3/2}c_\epsilon l} \tag{15}$$

with $Pr = \frac{K_m}{K_h} = \frac{S_m}{S_h}$ the turbulent Prandtl number. We then solve this equation through an implicit treatment of q assuming that the mean temperature and wind field does not vary much during the time step δt and thus keeping the explicit value - that is the value at the beginning of the time step - of Ri, S_m, Pr and l. Eq. 16 then reads:

$$\frac{q_{t+\delta t}-q_t}{\delta t} = \frac{lS_m}{\sqrt{2}}S^2\left(1-\frac{Ri}{Pr}\right) - \frac{q_{t+\delta t}^2}{2^{3/2}c_\epsilon l} \tag{16}$$

than can be rewritten in a second-order polynomial form after some rearrangement :

$$q_{t+\delta t}^2 + A_t q_{t+\delta t} + B_t = 0 \tag{17}$$

with $A_t = \frac{c_\epsilon l 2^{3/2}}{\delta t}$ and $B_t = -(\frac{q_t c_\epsilon l 2^{3/2}}{\delta t} + 2l^2 c_\epsilon S_m S^2(1-\frac{Ri}{Pr}))$

One can show that given the choice we will make for the formulation of the turbulent Prandlt number in the next section, Ri/Pr namely the flux Richardson number, is by construction always < 1. This in fact reflects a condition imposed by steady-state TKE budget

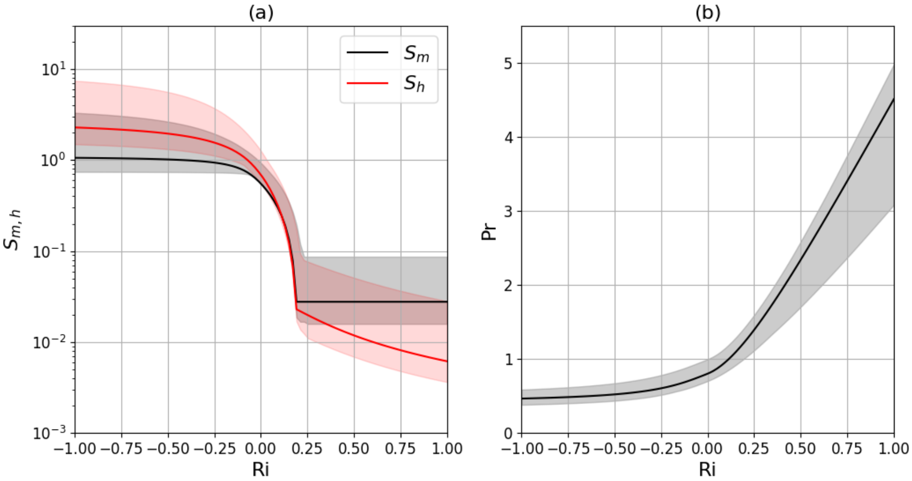

Figure 1. $S_{m,h}$ (panel a) and Pr (panel b) as functions of the Richardson number Ri following Eq. 20 and 23. Envelopes show the range of variation when adjustable parameters evolve in their range of acceptable values (Table 1). Solid lines show the curves for the following arbitrary set of parameters'values: $c_\epsilon = 5.9$, $Pr_n = 0.8$, $\alpha_{Pr} = 4.5$, $r_\infty = 2$, $Pr_\infty = 0.4$, $S_{min} = 0.05$ and $Ri_c = 0.2$.

equation for which the wind shear production term and the buoyancy term cannot exceed unity to maintain a non-zero TKE dissipation thus a non-zero turbulence (e.g, Zilitinkevich et al. (2008)).

The discriminant $\Delta = A_t^2 - 4B_t$ of Eq. 17 is thus always > 0 and the latter always admits a positive solution for q thus e that reads:

$$e = \frac{(-A_t + \sqrt{\Delta})^2}{8} \tag{18}$$

Step 2 The TKE variation due to the transport term $\mathcal{T}$ is then calculated and added to the value found in step 1. The calculation of this term consists in resolving the following equation:

$$\frac{\partial e}{\partial t} = \frac{1}{\rho}\frac{\partial}{\partial z}\left(\rho K_e \frac{\partial e}{\partial z}\right) \tag{19}$$

With an *a priori* knowledge of K_e - namely an explicit value of K_e calculated with the e value from Step 1 - Eq 19 is a typical diffusion equation that is solved implicitly in time through a tri-diagonal matrix inversion (Dufresne & Ghattas, 2009).

2.3 Heuristic expressions for the stability functions and turbulent Prandtl number

We now have to derive a heuristic expression for the stability function S_m of the gradient Richardson number $Ri = N^2/S^2$ to be used in the formulation of the diffusion coefficient for momentum. On one hand, S_m should increase when an atmospheric layer locally becomes more unstable and thus with decreasing negative Ri. On another hand, we want to prevent S_m from reaching infinite value when $Ri \to -\infty$ to avoid risk of numerical instabilities when $K_m \to \infty$ (Lenderink & Holtslag, 2000). It is worth recalling here that in unstable conditions, turbulent transport becomes non-local and another type of parameterization such as a mass-flux scheme should come in support of the K-diffusion. In stable conditions as turbulent mixing intensity decreases with increasing stability, we assume a simple linear decrease with Ri down to a minimum value attained when the Richardson number equals a critical value (Mellor & Yamada, 1974).

Following Lenderink and Holtslag (2004), we propose the following expression for S_m plotted in Figure 1a:

$$S_m(Ri) = \begin{cases} c_n + \frac{2}{\pi}(c_\infty - c_n)\arctan(\frac{-Ri}{Ri_0}) & \text{if Ri} < 0 \\ \max\left(c_n(1 - \frac{Ri}{Ri_c}), S_{min}\right) & \text{if Ri} \geq 0 \end{cases} \tag{20}$$

c_n is the value of S_m at $Ri = 0$ and c_∞ is the S_m value in the convective limit. $r_\infty = c_\infty/c_n$ is comprised between 1.2 and 5 (Mellor & Yamada, 1982; Lenderink & Holtslag, 2004). Ri_c is a critical Richardson number whose inverse value controls the slope of S_m in stable conditions. Previous literature suggests Ri_c values comprised between 0.19 and 0.25 (Mellor & Yamada, 1974, 1982; He et al., 2019). As the turbulence vertical anisotropy does not reach 0 in very stable conditions (Zilitinkevich et al., 2007; Li et al., 2016), S_m must be lower-bounded by a value S_{min} which is roughly around 0.05 and that we will make vary between 0.025 and 0.1.

The continuity in slope for $Ri = 0$ further gives:

$$Ri_0 = \frac{2}{\pi}(c_\infty - c_n)\frac{Ri_c}{c_n} \tag{21}$$

Furthermore, the so-called local-scaling similarity theory in stable boundary layers (Nieuwtsadt, 1984; Derbyshire, 1990; van de Wiel et al., 2010) implies that in stationary conditions, turbulent fluxes and vertical gradient wind speed must scale such that $\frac{K_m}{lS^2}$ converges towards 1 in the neutral limit. This conditions leads to a direct relationship between c_n and the coefficient c_ϵ (Baas et al., 2018; He et al., 2019), the latter being the ratio between the mixing length l and the TKE dissipation length scale (Sect. 2.2.1):

$$c_n = c_\epsilon^{-1/3} \tag{22}$$

The stability function for the heat flux S_h is estimated through a parametrization of the turbulent Prandtl number Pr. Under unstable conditions, the dominant coherent structures such as rising plumes and thermals have vertical velocity anomalies which generally better correlate with buoyancy and temperature anomalies than momentum anomalies in average. Therefore, one expects Pr to decrease with increasing instability (Li, 2019). In stably stratified conditions, buoyancy is expected to suppress the transport of heat but the existence of gravity waves can maintain some transport of momentum inducing an increase in Pr with increasing stability. Collection of field experiments, laboratory data and LES and DNS results shows a consistent increase in Pr with Ri with a asymptotical linear behaviour at strong stability (Zilitinkevich et al., 2008; Li, 2019). We therefore propose the following expression of Pr that is plotted in Figure 1b:

$$Pr(Ri) = \begin{cases} Pr_n - \frac{2}{\pi}(Pr_\infty - Pr_n)\arctan(\frac{-Ri}{Ri_1}) & \text{if Ri} < 0 \\ Pr_n e^{\frac{1-\alpha_{Pr}}{Pr_n}Ri} + \alpha_{Pr} Ri & \text{if Ri} \geq 0 \end{cases} \tag{23}$$

The formulation in stable conditions is inspired from Venayagamoorthy and Stretch (2010) and it shows fair agreement with experimental data (Li, 2019). α_{Pr} is the slope of the asymptotical linear trend at high stability and its value ranges from 3 to 5 (Grisogono, 2010). Pr_n is the neutral value of Prandtl number which from extensive laboratory and field experiments as well as theoretical works range from 0.7 to 1 (Grisogono, 2010; Li, 2019). The continuity in slope at $Ri = 0$ gives

$$Ri_1 = \frac{2}{\pi}(Pr_\infty - Pr_n) \tag{24}$$

Pr_∞ is the value of Pr in the convective limit and its value roughly ranges between 0.3 and 0.5 (Li, 2019).

2.4 Vertical turbulent mixing length formulation

In near-neutral conditions, we choose a turbulent vertical length-scale formulation l_n similar to Blackadar (1962) in which the displacement of eddies is limited by the distance to the ground in the neutral limit:

$$l_n = \frac{\kappa z l_\infty}{\kappa z + l_\infty} \tag{25}$$

where κ is the Von Kármán constant. l_∞ is the mixing-length far above the ground whose value in near-neutral conditions is generally estimated between 15 and 75 m (Sun, 2011; Lenderink & Holtslag, 2004) In stable conditions, the vertical displacement of eddies - whose size is roughly above the so-called Ozmidov scale - is limited by the stratification of the flow (e.g. van de Wiel et al. (2008)). André et al. (1978) and Deardoff (1980) introduced a widely used buoyancy length-scale which depends on the flow stratification characterised by Brunt-Väisälä pulsation N. The mixing length in stable conditions l_s then read :

$$l_s = c_l \frac{\sqrt{e}}{N} \tag{26}$$

c_l being a scalar whose value varies between 0.1 and 2 (Deardoff, 1980; Nieuwtsadt, 1984; Grisogono & Belušić, 2008; Baas et al., 2018).

More recent studies introduced wind-shear dependent formulation of l_s to account for the deformation of eddies - whose size is above a so-called Corrsin scale - by vertical wind shear (e.g. Grisogono and Belušić (2008); Grisogono (2010); Rodier et al. (2017)). Grisogono and Belušić (2008) proposed a mixing-length formulation including both the effect of stratification and vertical wind shear S^2 that reads:

$$l_s = c_l \frac{\sqrt{e}}{2\sqrt{S^2}(1 + \sqrt{Ri}/2)} \tag{27}$$

The final mixing-length l, being either ground-limited or stratification-limited is the minimum between l_n and l_s. In the model implementation, we choose a commonly-used continuous interpolation formulation:

$$l = \left(\frac{1}{l_n^\delta} + \frac{1}{l_s^\delta}\right)^{-1/\delta} \tag{28}$$

$\delta = 1$ by default. The two expressions of l_s can be used independently in the parameterization but unless otherwise stated, the results presented in the rest of the paper have been obtained with formulation dependent on both stratification and wind shear (Eq. 27). In practice, l is also lower bounded by a value $l_{min} = 1$ cm to prevent it from reaching value below the Kolmogorov length scale in planetary atmospheric motions (Chen et al., 2016). As l_s depends on the TKE, in practice l is calculated with an explicit value of the TKE i.e. the value at the beginning of the time-step.

2.5 Surface layer scheme matching

Neglecting the vertical diffusion term of TKE $\mathcal{T}$, Eq. 7 in stationary conditions ($\partial_t e = 0$) can be re-arranged to give a first-order turbulent closure like expressions of the eddy diffusion coefficients for momentum and heat (Cuxart et al., 2006):

$$K_m = l^2 \sqrt{S^2} F_m(Ri) \tag{29}$$

$$K_h = l^2 \sqrt{S^2} F_h(Ri) \tag{30}$$

where

$$F_m(Ri) = S_m^{3/2} \sqrt{c_\epsilon} \left(1 - \frac{Ri}{Pr}\right)^{1/2} \tag{31}$$

$$F_h(Ri) = S_m^{7/4} Pr^{-1} \sqrt{c_\epsilon} \left(1 - \frac{Ri}{Pr}\right)^{1/2} \tag{32}$$

are first-order like stability functions. Near the ground in the surface layer, $l \approx \kappa z$ and England and McNider (1995) then show that $F_{m,h}$ functions are identical to the stability functions involved in the bulk expressions of the surface drag coefficients used to calculate surface fluxes of momentum and heat in models :

$$C_{m,h} = \frac{\kappa^2}{\log(z/z_{0m})\log(z/z_{0m,h})} F_{m,h} \tag{33}$$

with z_{0m} and z_{0h} the surface roughness lengths for momentum and heat respectively. Provided turbulence in the surface layer can be assumed to be close to a stationary state, using the same formulations for S_m and Pr in both the turbulent diffusion and surface layer schemes leads to a fully consistent formulation of turbulent fluxes from the surface layer up to the top of the boundary-layer.

2.6 Degrees of freedom of the scheme and adjustable parameters

Table 1 summarises all the 10 adjustable parameters of the new parameterization and their ranges of acceptable values as previously introduced in the text. The 8 first parameters in bold are those affecting the simulation of the neutral and stable boundary layers and taken into account in the tuning phase in the next section. It is worth mentioning that we also lower-bound the turbulent diffusion coefficients with the kinematic molecular viscosity and conductivity of the air, which are not tuning parameters per se but pressure and temperature dependent - thus planet dependent - quantities.

3 Implementation in General Circulation Models, evaluation and tuning

3.1 Implementation in the LMDZ GCM and Mars Planetary Climate Model

The ATKE parameterization has been implemented in the LMDZ Earth GCM (Hourdin et al., 2020; Cheruy et al., 2020), atmospheric component of the French IPSL Coupled-Model (Boucher et al., 2020) involved in the Coupled Model Intercomparison Project (CMIP) exercices. The turbulent-mixing parameterization of LMDZ has received a lot of attention in the past two decades, particularly regarding the convective boundary layer and the very stable boundary layer. It is a hybrid scheme in the sense that turbulent fluxes are expressed as a sum of a K-diffusion term - from the TKE-l scheme of Yamada (1983) and revisited in Hourdin et al. (2002) and Vignon, Hourdin, et al. (2017) - and a non-local transport term by convective plumes (Rio et al., 2010; Hourdin et al., 2019). Despite those efforts, recent tests revealed that the latest version of the model - the CMIP6 version - still exhibits numerical instabilities in near-neutral boundary layers in presence of strong wind shear.
As a proof of concept, the ATKE scheme has also been implemented in the Mars Planetary Climate Model (Mars PCM, Forget et al. (1999)). This model also uses a hybrid scheme

Table 1. Name, definition and range of acceptable values for the adjustable parameters. Parameters are dimensionless exception l_∞ which is a length in m. Parameters in bold are those which affect the simulation of the neutral and stable boundary layer.

Name	Definition	Range
$\mathbf{c_\epsilon}$	controls the value of the dissipation length scale	[1.2 - 10]
$\mathbf{c_e}$	controls the value of the diffusion coefficient of TKE	[1 - 5]
$\mathbf{l_\infty}$	asymptotic mixing length far from the ground	[15 - 75]
$\mathbf{c_l}$	controls the value of the mixing length in stratified conditions	[0.1 - 2]
$\mathbf{Ri_c}$	critical Richardson number controlling the slope of S_m in stable conditions	[0.19 - 0.25]
$\mathbf{S_{min}}$	minimum value of S_m in very stable conditions	[0.025 - 0.1]
$\mathbf{Pr_n}$	neutral value of the Prandtl number	[0.7 - 1]
$\boldsymbol{\alpha_{Pr}}$	linear slope of Pr with Ri in the very stable regime	[3 - 5]
r_∞	ratio between c_∞ and c_n controlling the convective limit of S_m	[1.2 - 5.0]
Pr_∞	value of Pr in the convective limit	[0.3 - 0.5]

with a TKE-l diffusion scheme inspired from Yamada (1983) and a dry parameterization of convective plumes (Colaïtis et al., 2013). Colaïtis et al. (2013) have pointed out that the default TKE-l scheme of Hourdin et al. (2002) leads to numerical oscillations in strongly stratified Martian nighttime conditions. They addressed this issue by imposing a minimum mixing coefficient K_{min} whose value depends on the boundary layer height following Holtslag and Boville (1993).

3.2 Parametric sensitivity of the ATKE scheme and tuning

3.2.1 Initial test on the GABLS1 case and parametric sensitivity

The ATKE scheme is first tested on single column simulations using the 1D version of LMDZ with a 95-level vertical grid introduced in Hourdin et al. (2019). We run 1D simulations on the GEWEX Atmospheric Boundary Layer Study 1 (GABLS1) single column model intercomparison exercise. The latter consists in a no-radiation idealized 9 hour simulation of the development of a weakly stable boundary layer, with a constant zonal geostrophic wind of 8 m s^{-1} and a constant surface cooling of -0.25 K h^{-1} (Cuxart et al., 2006). The fair convergence of 3D LES on this case - with the exact same initial and boundary conditions as those for single column models - make LES suitable references for GABLS1. Nonetheless, to sample the small variability between LES runs, we consider hereafter 5 reference LES which correspond to the MO-1m, MO-2m, UIB-2m, IMUK-1m, IMUK-2m simulations listed in Table 2 of Beare et al. (2006), the suffix referring to the vertical resolution.

Given the ranges of acceptable values associated with each of the $n = 8$ free parameters affecting the simulation of the stable boundary layer listed in Table 1, we need to run simulations with different sets of parameters to assess the parametric sensitivity of the scheme. For this purpose, we use the HighTune explorer statistical tool originally developed in the Uncertainty Quantification community and now applicable in atmospheric modeling (Couvreux et al., 2021). This tool allows to make a first perturbed physics ensemble experiment through an exploration of the initial n-dimension hypercube of parameters defined by the intervals given in Table 1 using a Latin Hyper Cube sampling method. Here 80 (10 times n) sets of parameters or free parameters' vectors are sampled. Unless otherwise stated, the simulations are run with a 15 min time step, i.e. the typical value used for the LMDZ physics and that used for the ensemble of CMIP6 simulations.

Figure 2 shows the results of this *a priori* sensitivity analysis to free parameters' values for the vertical profiles of potential temperature, wind speed and TKE averaged over the

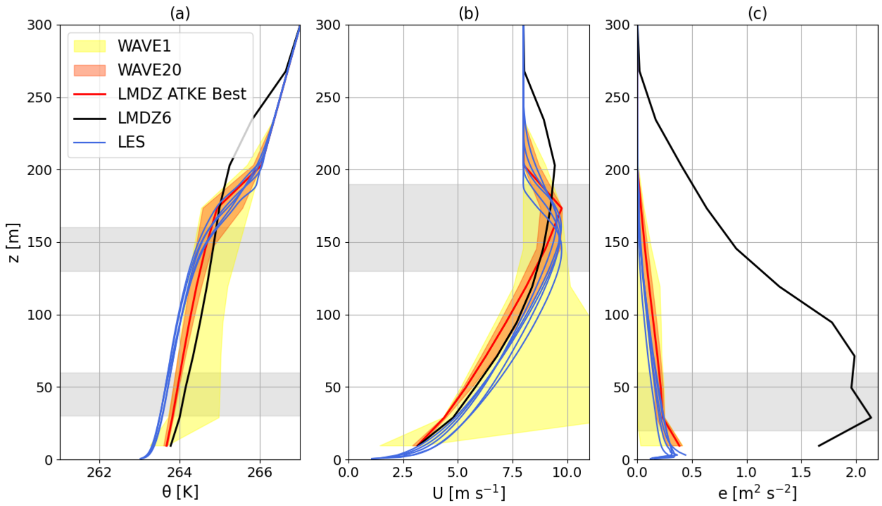

Figure 2. Evolution of envelopes of the vertical profiles of potential temperature (panel a), wind speed (panel b) and TKE (panel c) after 9 hours of GABLS1 simulation. Yellow and orange envelopes correspond to waves 1 and 20 respectively i.e. to the 1st and 20th set of 80 simulations during the tuning exercise. Blue curves show the 5 reference LES. The red curve shows the 'best' LMDZ simulation. The black curve shows the CMIP6 version of LMDZ for comparison. The horizontal light grey band show the vertical ranges over which the metrics are calculated for each variable. In panel c, note that the full (resolved+subgrid) TKE from the LES is shown.

eighth hour of the simulation. The yellow envelope displays the variability (minimum and maximum values) amongst the 80 simulations from this first so-called 'wave' of simulations. Albeit encompassing the five reference LES coming from the GABLS1 LES intercomparison exercise (Beare et al., 2006), this yellow envelope hightlights the large range of vertical profiles obtained. This is a signature of the high sensitivity of the results to the parameters as they are varied accross the range given in Table 1. In particular, very strong and unrealistic momentum decoupling manifesting as very strong wind speed gradient near the surface is allowed by the scheme in regions of the parameter space where the negative feedback of the wind shear on the mixing length (Eq. 27) is overappreciated. Interestingly, Figure 3b shows that such a decoupling is never simulated when using the buoyancy-only dependent length scale (Eq. 26). However, even if the yellow envelop is reasonable for the potential temperature and wind speed (Figure 3a,b), the use of the buoyancy-only dependent length scale can lead to unrealistically strong values of TKE in the middle of the boundary layer (Figure 3c) owing to overly high mixing length values.

Overall, the large width of the yellow envelop in Figure 2 and the possible large discrepancy with respect to the LES call for a reduction of the parameter space and a calibration of the ATKE scheme.

3.2.2 History matching with iterative refocusing

For this purpose, we follow a history matching with iterative refocusing procedure which in practice is performed with HighTune explorer. This procedure is made of 6 steps and is fully described in Couvreux et al. (2021) and Hourdin et al. (2021). We refer the

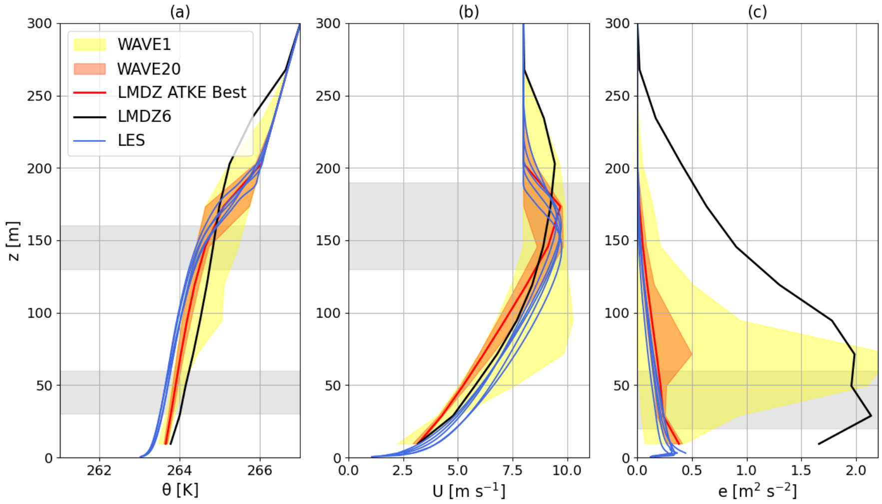

Figure 3. Same as Figure 2 but for simulations using the buoyancy length-scale formulation (Eq. 26) instead of the stratification and wind-shear dependent formulation (Eq. 27) in stable conditions.

reader to the aforementioned papers for details on the method and describe here the main steps for our application.

Step 1 We first define 5 metrics, i.e. targets for the model with respect to the LES reference, to properly capture the boundary layer structure. Those metrics are the potential temperature at the bottom (average between 30 and 60 m) and top (average between 130 and 160 m) part of the boundary layer, the zonal wind speed at the low-level jet height (average between 130 and 190 m) and the TKE at the bottom (average between 20 and 60 m) and middle (average between 60 and 100 m) part of the boundary layer. All metrics are calculated on hourly-mean profiles between the 8th and 9th hour of the simulation, when the stable boundary layer is well developed.

Step 2 We then define the initial parameter space consisting in a 8-dimension space corresponding to the 8 parameters in bold in Figure 1 and their associated range of possible values.

Step 3 This parameter space is then sampled 80 times and experimented on GABLS1 simulation as in Sect. 3.2.1.

Step 4 Based on those 80 simulations, an emulator is built for each metric based on a Gaussian Process providing values for the expectation and variance at any location in the parameter space.

Step 5 We then compare the simulated metrics with respect to those from the LES reference through the calculation of an implausibility I for each metrics at each point λ of the parameter space:

$$I(\lambda) = \frac{|r - E[e_m(\lambda)]|}{\sqrt{\sigma_r^2 + \sigma_d^2 + Var(e_m(\lambda))}} \tag{34}$$

where the numerator is the absolute difference between the reference metrics r and the corresponding expectation from the emulator $E[e_m(\lambda)]$; and the denominator is the standard deviation of this difference, which includes the reference uncertainty (i.e. the spread between LES σ_r^2), the uncertainty associated to the emulator ($Var(e_m(\lambda))$), and model structural uncertainty (σ_d^2, see Couvreux et al. (2021) for details). As the latter is not a priori known, one has to prescribe an arbitrary 'tolerance to error' (see thorough discussion on the rationale behind this tolerance in Hourdin et al. (2021)) that we set to 0.25 K for potential temperature, 0.25 m s^{-1} for wind speed and 0.01 m^2 s^{-2} for TKE. History matching then rules out a part of the parameter space that corresponds to unacceptable model behaviour - i.e. with an implausibility higher than a given cut-off value of 3 - and keeps a not-ruled out yet (NROY) space.

Step 6 Iterative refocusing then consists in sampling 80 new free parameter vectors in the NROY space and reiterates over several tuning 'waves' from step 4 to 6.

Note that this procedure is not an optimization method providing in the end a single set of parameters, but a method ruling-out a non-plausible part of the initial parameter space and giving the space of acceptable free parameters - given the chosen metrics and tolerances - once it has converged.

The results after 20 waves of tuning are shown with orange envelopes for the potential temperature, wind speed and TKE profiles in Figure 2. Compared to the initial and first wave (yellow envelopes), one can first notice the convergence towards LES curves. Considerable improvement is obtained with respect to the CMIP6 version of LMDZ, with a shallower and more realistic - compared to LES - boundary-layer height, a more peaked low-level jet and lower and much closer-to-LES TKE values. Nonetheless, the potential temperature (resp. wind speed) in the first tens of meters above the surface remains slightly overestimated (resp. underestimated). Such biases can be reduced by adding metrics targeting the lowermost part of the profiles and increasing the vertical resolution close to the surface (not shown).

We now examine the 10 'best' simulations obtained during the tuning exercise. The adjective 'best' is employed here as in Hourdin et al. (2021) in the sense that the maximum (across metrics) value of the ratio of the distance to LES divided by the tolerance to error is the smallest at the end of the tuning exercise. Note that this choice of 10 simulations and the denomination 'best' goes beyond the history matching philosophy as there is *a priori* no reason to prefer specific configurations than others in the final NROY spaces given the chosen metrics and tolerances. A choice is done here to illustrate the behaviour of the ATKE scheme for single sets of parameters obtained at the end of the tuning process in 1D and 3D simulations.

Figure 4a,c) show that they reproduce fairly well the profiles of heat and momentum turbulent fluxes, i.e. two quantities that were not directly targeted during the tuning. $K_{m,h}$ values are also much lower than those in the CMIP6 physics simulation (Figure 4b,d) which concurs with conclusions regarding the profiles of TKE in Figure 2c. In addition, Figure 5 reveals the good numerical stability and convergence properties of the TKE in these simulations, as well as the considerable improvement regarding these aspects with respect to the CMIP6 version of the LMDZ physics. This makes us confident with the robustness and efficiency and the numerical resolution method for the TKE evolution equation presented in 2.2.2.

When inspecting more deeply the NROY space after 20 waves of tuning (Figure 6), one can notice that its final shape has been mostly constrained by the c_l and c_ϵ, and to a lesser extent by l_∞. This does not absolutely mean that the other 5 parameters do not play role in the overall behaviour of the scheme but this shows that the representation of the GABLS1 weakly stable boundary layer with ATKE mostly depends upon the value of c_l, c_ϵ and l_∞. This point is further shown by the strong similarity between Figure 7 - which has been produced with a tuning on c_l, c_ϵ and l_∞ only - and Figure 2. Such a result is not that surprising since the turbulent diffusion in weakly stable boundary layer mostly results from

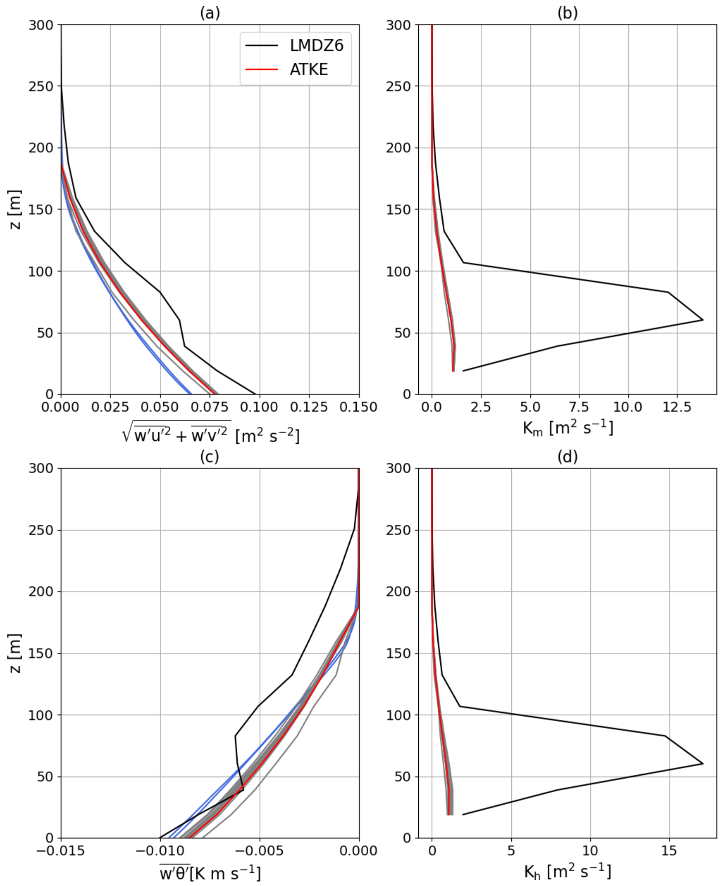

Figure 4. Vertical profiles of momentum flux (panel a), heat flux (panel c) , eddy diffusivity coefficient for momentum (panel b) and heat (panel d) after 9 hours of GABLS1 simulation. Grey curves show the LMDZ simulations run with the 10 best parameter vectors after the tuning exercise. Blue curves in panels a and c show the 5 reference LES. The red curve shows the 'best' LMDZ simulation obtained during the tuning exercise (see main text for details). The black curve shows the CMIP6 version of LMDZ for comparison.

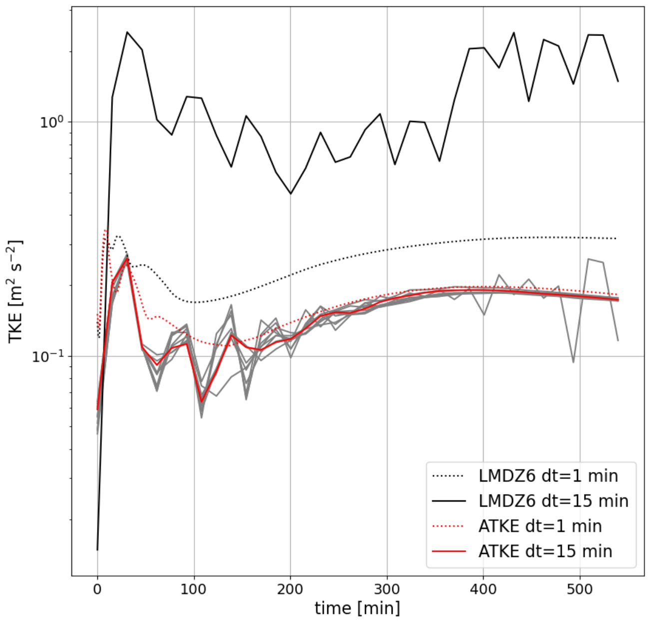

Figure 5. Time evolution of the TKE at 40 m a.g.l. in LMDZ single column model GABLS1 simulations. Solid grey curves show the simulations run with the 10 best parameter vectors after the tuning exercise and a 15 min time step. The solid and dotted red curves shows simulations run with the best parameter vector and a time step of 15 and 1 min respectively. The solid and dotted black curves shows simulations run with CMIP6 version of LMDZ and a time step of 15 and 1 min respectively.

eddies whose size and energy are controlled by wind shear intensity and TKE dissipation. In addition, the weak dependence upon c_e may have somewhat been expected given the relatively weak contribution of the transport term $\mathcal{T}$ is the overall TKE budget (not shown). Regarding S_{min}, Ri_c and α_{Pr}, one may expect a more important role of those parameters in very stable boundary layers i.e. with a stratification more pronounced compared to that in GABLS1. Their values might thus be more constrained if we were to tune the ATKE scheme over a more stable boundary layer case such as GABLS4 (Couvreux et al., 2020) instead of or in addition to GABLS1. However LES do not converge that well on GABLS4 which makes the tuning exercise more delicate. Moreover, the role of radiation in determining the structure of the boundary-layer becomes increasingly important as stability increases (Edwards, 2009) and in addition to turbulent diffusion, the coupling between turbulence and radiation becomes an essential feature to capture with models. We therefore leave this aspect for further research.

3.3 Challenging the Antarctic and Martian stable boundary layers

We now conduct two short and arbitrary applications of the ATKE parameterization in simulations with the LMDZ GCM and Mars PCM.

3.3.1 Stable boundary layer regimes at Dome C, Antarctic Plateau

First, we verify that the proposed scheme is able to reproduce the dichotomous behaviour of the stable boundary layer at Dome C on the Antarctic Plateau that is, a very stable regime with strong temperature surface-based inversions and collapsed turbulence versus a weakly stable state with weak inversions. The sharp transition between those 2 regimes occurs in a narrow range of wind speed (Vignon, van de Wiel, et al., 2017; Baas et al., 2019). Such a test was proposed in Vignon et al. (2018) to verify the ability of the CMIP6 version of LMDZ to reproduce the overall dynamics of the stable boundary layers and it is performed here as capturing the Dome C boundary layer was identified as a *target* during the development of LMDZ for CMIP6 (Cheruy et al., 2020). This is an aspect that we want to conserve throughout the development of the LMDZ physics and particularly when introducing a new turbulent diffusion scheme. It is also worth noting that such a test was also used for the recent development of the CanAM model (He et al., 2019) as well as for verifying the robustness of LES of the stable boundary layer (van der Linden et al., 2019). We follow here the exact same LMDZ simulation configuration as in Vignon et al. (2018) that is, one year (2015) simulations are conducted with the zooming capability of the LMDZ to refine a 64×64 global grid to reach a 50×50 km on the Dome C. One slight difference though with respect to Vignon et al. (2018) is that we use the 95-level vertical grid used in the previous section instead of the 79-level grid in the reference paper. Nudging in wind, temperature and humidity towards ERA5 reanalyses (Hersbach et al., 2020) is applied outside the zoom area to evaluate the sub-components of the physics of the model apart from likely deficiencies in representing the large scale meteorological fields. The reader is referred to Vignon et al. (2018) for details on the simulation configuration as well as the surface snow treatment in LMDZ. The simulation has been run with the CMIP6 version of the LMDZ physics as well as by an adapted versions using the ATKE diffusion scheme and the 10 'best' sets of parameters found from the single column model tuning.

A simple diagnostics to assess the representation of the two stable boundary layer regimes is to investigate the dependence of the surface-based temperature inversion upon the wind speed in clear sky conditions. Data align along a well-defined 'inverted-S' shape curve (Vignon, van de Wiel, et al., 2017; van de Wiel et al., 2017), the two horizontal branches corresponding to the two regimes and the vertical one to the non-linear transition between them as the wind speed increases or decreases (Figure 8a). As shown in Figure 8b, the CMIP6 version of LMDZ reasonably captures the strong surface-atmosphere decoupling in very stable conditions and the 2-regime behaviour. LMDZ with the ATKE scheme run with the 'best' set of parameters (Figure 8c) retained in Sect. 3.2 reproduces even more

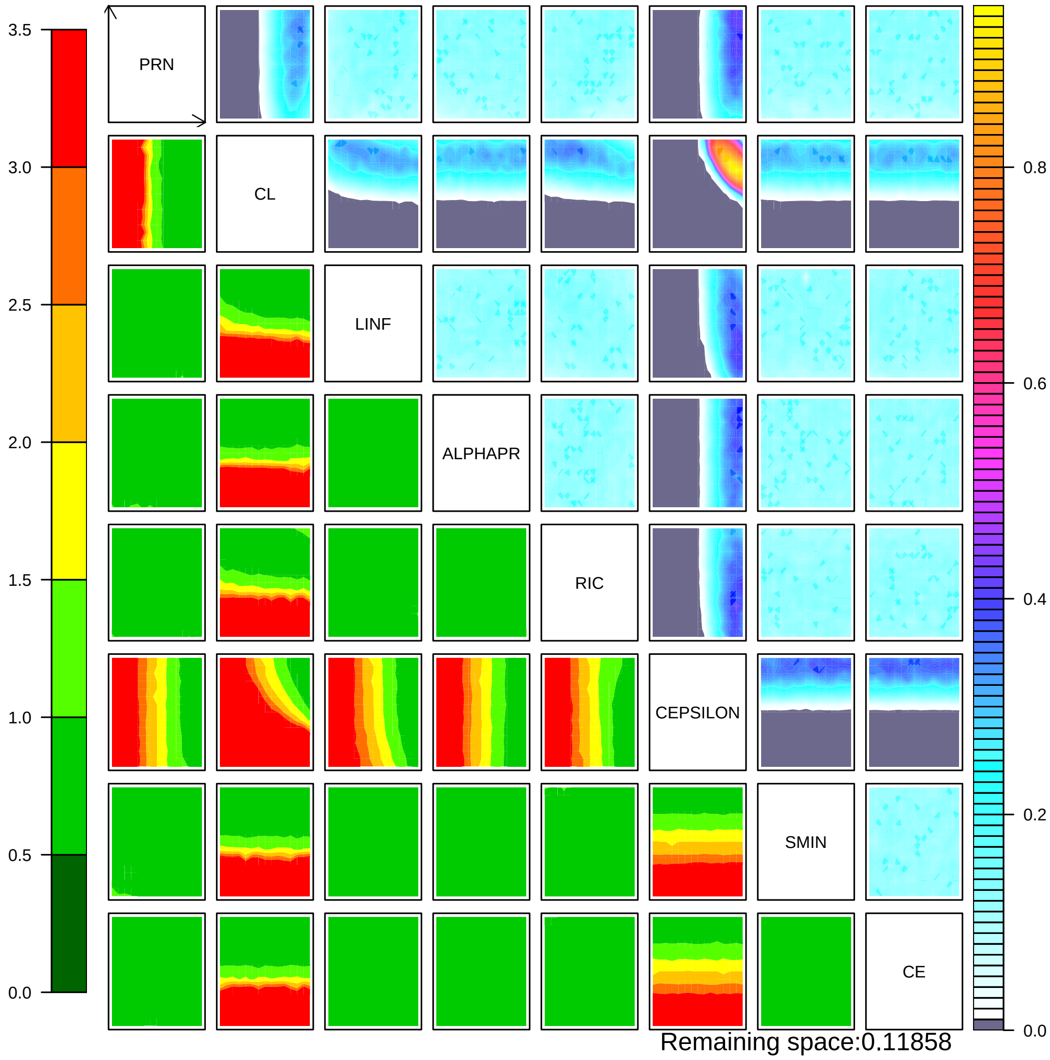

Figure 6. Implausibility matrix after 20 waves of history matching exploration. The upper-right triangle is made of sub-matrices that show the fraction of points with implausibility lower than the chosen cutoff while the sub-matrices of the lower-left triangle show the minimum value of the implausibility when all the parameters are varied except those used as x- and y-axis, the name of which are given on the diagonal of the main matrix. The number at the bottom of the graph shows the NROY space value (fraction of the initial parameter space) after 20 waves.

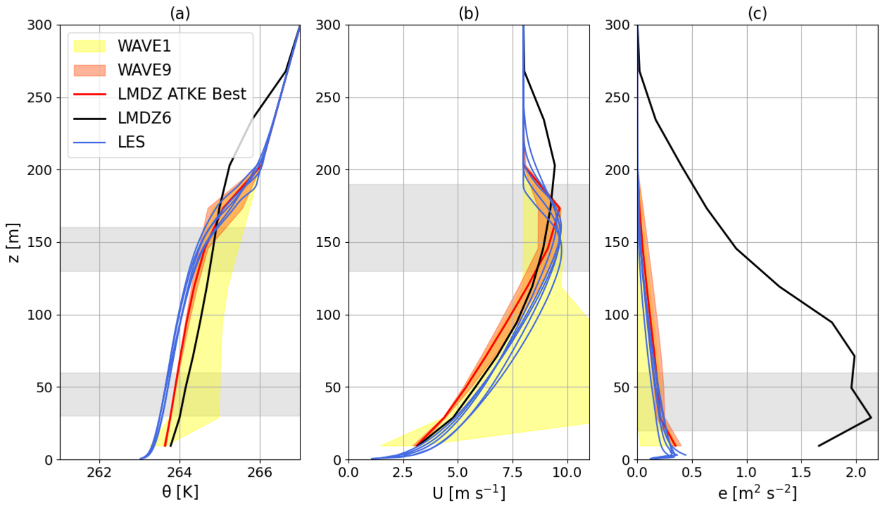

Figure 7. Same as Figure 2 but after a tuning on c_ϵ, c_l and l_∞ only. The other parameters have been arbitrarily set to the following values: $Ri_c = 0.2$, $S_{min} = 0.05$, $Pr_n = 0.8$, $\alpha_{Pr} = 4.5$ and $c_e = 2.0$. Note that we have stopped the tuning expercice at the 9th wave here since convergence has been attained.

realistically reproduce the 2-regime behaviour - that is, the reversed 'S' shape pattern - and the decoupling in very stable conditions despite an overestimation of the strong temperature inversions. The latter can be attributed to an overly weak downward longwave radiative flux from the very dry and cold Dome C atmosphere in clear-sky conditions (Vignon et al., 2018).

An important point here is that such results are obtained with all the 10 'best' sets of parameters after 20 waves of tuning on GABLS1 (Figures 8c-l) and despite the fact that such a GABLS1-based tuning has not substantially constrained parameters that may be *a priori* important in very stable conditions such as S_{min}, Ri_c and α_{Pr}. In fact, the transition between the weakly and very stable regimes of the stable boundary-layer primarily relies on the ability of a TKE-l scheme to allow for a turbulence collapse in very stable conditions (Vignon et al., 2018). This is the case with the ATKE scheme - whatever the S_{min}, Ri_c and α_{Pr} value chosen in their corresponding ranges of acceptable values - as no artificial threshold or lower-bound has been prescribed to maintain a certain amount of TKE in very stable conditions.

3.3.2 Nocturnal stable boundary layer collapse on Mars

Mars has a thinner and much less dense atmosphere compared to Earth and its planetary boundary layer exhibits stronger diurnal variations (Spiga et al., 2010b; Petrosyan et al., 2011) with a abrupt collapse at the day-night transition. During night-time, the Martian boundary layer exhibits numerous similarities with that of the polar regions on Earth such as strong surface-based temperature inversions associated with very weak turbulence (Banfield et al., 2020), the latter being able to re-activate through wind shear production associated with low-level jets (Chatain et al., 2021).

This extreme environment enables us to challenge the versatility of ATKE parameterization and compare its performance with the default TKE-l scheme used in the current Mars PCM (Colaïtis et al., 2013).

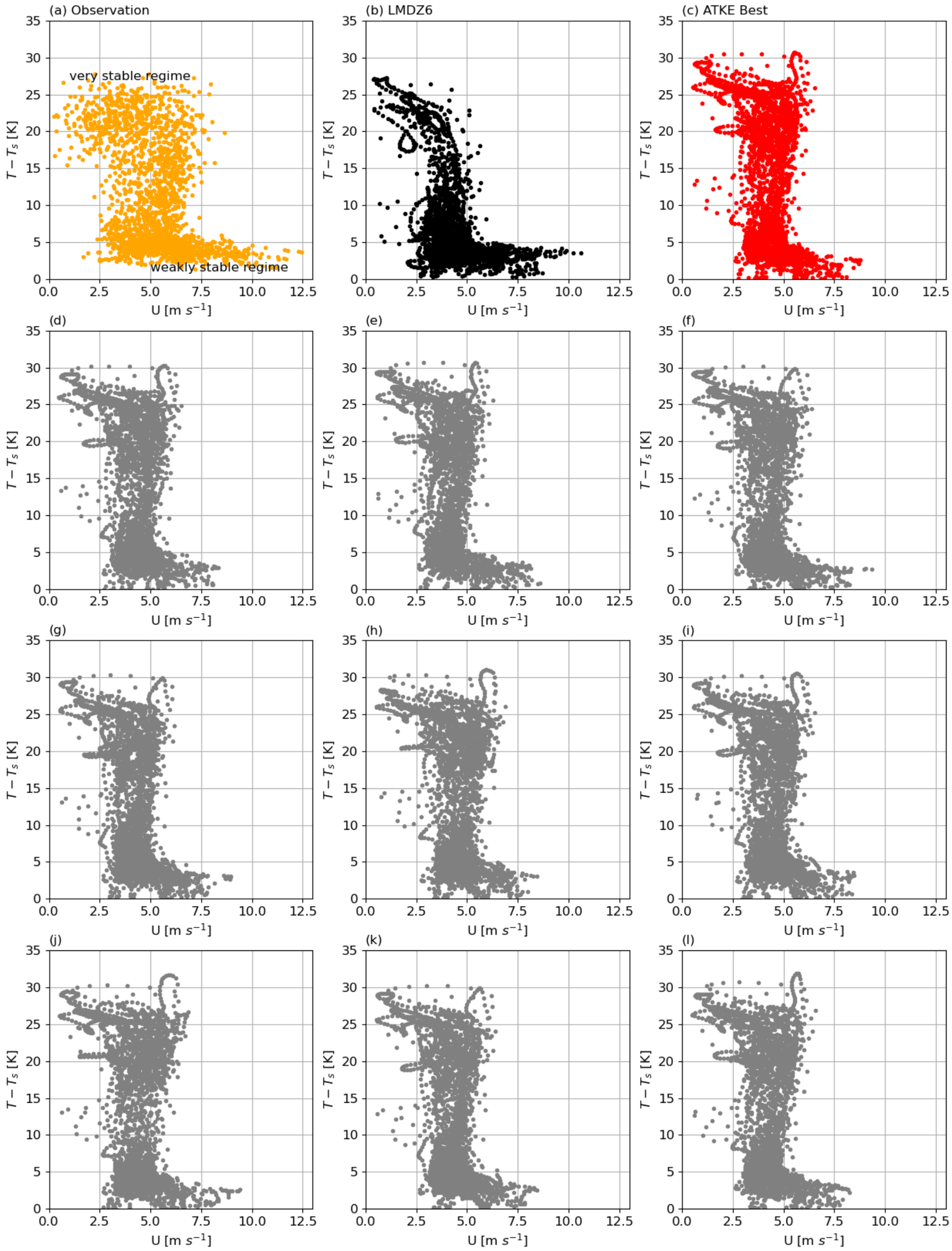

Figure 8. Temperature inversion between 10 m and the ground surface plotted as a function of the 10-m wind speed in clear-sky conditions (downward longwave radiative flux < 100 W m^{-2}) from April to September 2015. Panel a shows results from in situ observations. Panel b (resp. c) show the LMDZ simulation in the CMIP6 physics configuration (resp. with the ATKE scheme using the best set of parameters retained in Sect. 3.2). Panels d to l show results from 9 simulations with the ATKE scheme using 9 following 'best' sets of parameters after the tuning phase on GABLS1. Dome C measurement data are from Genthon et al. (2021).

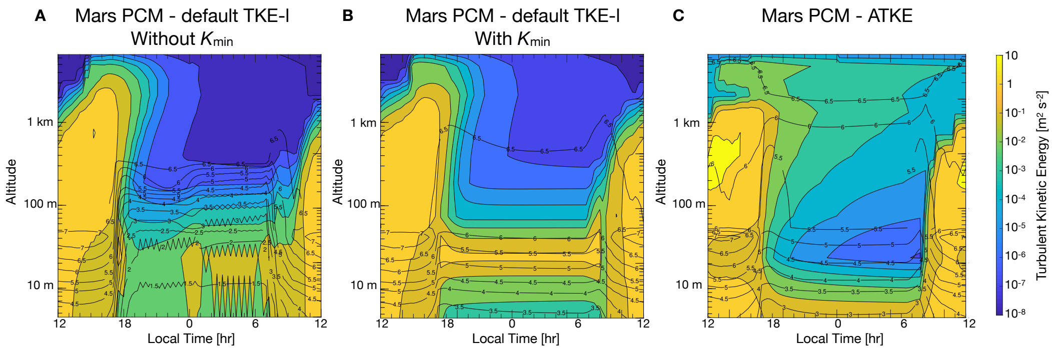

Figure 9. Evolution of the TKE through the Martian day in a) the baseline physics configuration; b) the same configuration with no minimum mixing coefficient K_{min}; c) the simulation using the ATKE scheme for turbulent diffusion. Black contours indicate the wind speed in m s^{-1}.

As a first test, we compare the two parameterizations using the single-column version of the Mars PCM to assess the overall behaviour of the diurnal cycle of the boundary layer and the numerical stability of the model. The single-column version of the Mars PCM uses the same physics as the 3D model (Lange et al., 2023) and a vertical grid with 6 levels in the first km above the ground. No lateral advection of heat and momentum is prescribed, the initial temperature profile is set to 180 K and the zonal wind speed is nudged towards a constant value of 7 m s^{-1} which corresponds to values measured at the Mars Equator by the InSight lander (Banfield et al., 2020). Simulations are performed at the Equator, with no dust aerosols, and ran for several Martian days until the diurnal cycle reaches an equilibrium after 10 days. The nocturnal boundary layer simulated is weakly to moderately stable, with a near-surface gradient Richardson not exceeding 0.1. Figure 9 shows the evolution of the TKE (colour shading) and wind speed (contours) in the first km above the ground surface during a typical diurnal cycle. As explained in Sect. 3.1, the nocturnal TKE field simulated by the default TKE-l scheme of the Mars PCM is affected by strong numerical oscillations (Figure 9a) which are mitigated when adding a minimum mixing coefficient K_{min} (Figure 9b). When using the ATKE scheme with the 'best' set of parameters retained from the tuning on GABLS1 in Sect. 3.2.2 (Figure 9c) and with no prescription of K_{min}, the structure of the nocturnal boundary layer is well captured and no numerical oscillations affect the TKE and wind fields. Unlike in Figure 9b, the TKE exhibits a continuous decrease with increasing height in the nocturnal boundary layer, which better concurs with the typical TKE structure in weakly stable boundary layers (e.g., (Acevedo et al., 2015)).

We then assess the performance of the ATKE model by performing simulations with the 3D Mars PCM and comparing the results to in situ wind observations collected by the InSight lander deployed at a latitude 4.5° N and a longitude of 135° E. InSight continuously monitored the wind at a height of 1.2 m for almost one martian year with an unprecedented time resolution (Banfield et al., 2020). Two striking phenomena have been detected. First, a dramatic reduction of the wind speed, following the collapse of the boundary layer is observed around 17-18 local time during the clear season (Figure 10a) i.e., the first half of the Martian year when a relatively small amount of dust is present in the Martian sky (Kahre et al., 2017). The abruptness of this change is related to both the very low thermal inertia of the Martian ground surface and the thinness of the Martian atmosphere. Second, during the dusty season i.e. the second half of the Martian year, substantial night-time turbulence is observed (Chatain et al., 2021) and the decrease in near-surface wind speed is less pronounced (Figure 10d). Those two phenomena have been shown to be poorly

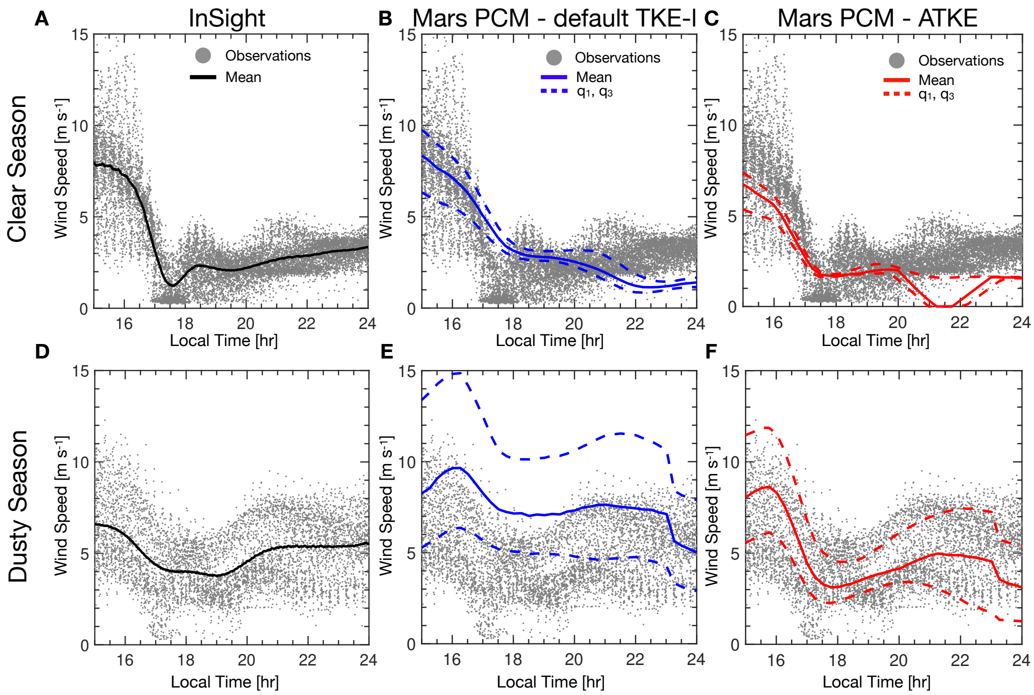

Figure 10. Comparison between InSight wind speed measurements (grey dots and black curves in panels a and d) and Mars PCM simulations using the default TKE-l scheme (b, e) and the ATKE scheme (c, f). For model fields, the mean wind speed over the period considered is presented in solid lines, and the diurnal variability is shown with the envelope of dashed lines (q_1 and q_3 referring to the first and third quartiles).

reproduced by the Mars PCM, in particular, the collapse of winds at sunset (Forget et al., 2021).

Here, as a proof of concept, we run the 3D Mars PCM using either the default TKE-l scheme and the ATKE scheme with the 'best' set of parameters from the GABLS1 tuning i.e. with no specific tuning for Martian conditions. Global simulations are performed over one complete martian year with a resolution of 3.75° in latitude and 135.9° in longitude. Initial conditions are derived from 10-year simulations which provide equilibrium states of water and CO_2 cycles (Pottier et al., 2017). The seasonal and geographic variations of dust opacity in the sky are prescribed using dust observations by (Montabone et al., 2015). Results are presented in Figure 10. Concurring with Forget et al. (2021), the model in its standard configuration fails to reproduce the sharp transition from high to low wind speeds at sunset (Figure 10b). This aspect is significantly improved when using the ATKE scheme (Figure 10c). However, the wind speed in the second part of the night remains underestimated in both configurations which questions the representation of the surface-atmosphere decoupling in this period (Chatain et al., 2021). In the dusty season, the current model overestimates the surface wind speed owing to an excess of turbulent mixing (Figure 10e), while the ATKE parameterization leads to more realistic wind speeds (Figure 10f).

Overall, this preliminary experiment demonstrates: i) the applicability of the ATKE parameterization on Mars and the promising results that can be obtained with a set of parameters not specifically tuned for Mars conditions and; ii) the improvement of the model both numerically and physically in stable conditions. Nonetheless, Mars simulations with the ATKE scheme would further benefit from a more adapted tuning using references such as Mars LES (Spiga et al., 2010a) or InSight observations (Banfield et al., 2020). It is also worth noting that the Mars atmosphere, particulaly at the poles i.e. far from the InSight landing site, exhibits particularities that cannot be properly captured with the current version of the ATKE scheme. A key aspect is that air buoyancy can be created by compositional vertical gradients of both water vapor and carbon dioxide, i.e. the prevailing gas of Mars' atmosphere. In particular, during the winter polar night, CO_2 condenses upon the ice cap surface (e.g., (Weiss & Ingersoll, 2000)) changing dramatically the near-surface atmospheric composition. Such an effect cannot be taken into account given with Brünt-Vaisala pulsation and Richardson number expressions based on a virtual potential temperature. This aspect deserves attention for further improvement of the ATKE scheme.

4 Summary and Conclusions

This study presents the development of a simple TKE-l parameterization of turbulent eddy coefficients for the simulation of the neutral and stable boundary layer in large-scale atmospheric models. The parameterization has been carefully designed such that all adjustable parameters have been clearly identified and their ranges of possible values defined to help the calibration and assess the parametric sensitivity. Instead of using fixed and empirical expressions of stability functions and turbulent Prandlt number, we have derived fully tunable and heuristic formulae to improve the versatility of the scheme and its potential applicability for planetary atmospheres composed of an ideal and perfect gas. A wind-shear and buoyancy dependent formulation for the mixing length in stratified conditions is considered. A 2-step numerical treatment of the TKE equation is further proposed and shows good convergence and stability properties at typical time steps used in large scale atmospheric models. The parametric sensitivity of the ATKE scheme has been assessed with the HighTune explorer tools using 1D simulations of the GABLS1 weakly stable boundary layer case with the single-column version of LMDZ. Using a History-Matching approach, we carried out a first calibration of the scheme allowing us to reduce the initial parameter space to keep an ensemble that satisfies the representation of weakly stable boundary layer. Substantial improvement with respect to the CMIP6 version of LMDZ has been achieved in terms of vertical profiles of temperature, wind, TKE and turbulent fluxes of momentum and heat, as well as in terms of numerical stability. However this tuning experiment restricted to the weakly stable GABLS1 case has not enabled us to clearly evidence a potential added value of a wind-shear and buoyancy dependent formulation for the mixing length in stratified conditions compared to a buoyancy only-dependent one, even if the vertical profile of TKE is slightly better captured.

The ability of the ATKE scheme to simulate the stable boundary layer as well as its applicability to planetary atmospheres have then been assessed through simulations of the Antarctic and Martian boundary layer with the LMDZ and Mars Planetary Climate model respectively. In particular the 2-regime behaviour of the stable boundary layer at Dome C, a challenge for turbulent diffusion schemes in GCMs, is reasonably well captured with the ATKE scheme. In addition, promising results have been obtained for the representation of the nocturnal Martian boundary layer with improvements regarding the numerical stability compared to the original model. Such results pave the way for a Mars-specific tuning of the ATKE scheme in the future.

A prospect of our work is to verify the physical and numerical robustness of the ATKE parameterization in atmospheric flows with extremely strong wind shear such as katabatic winds developing over ice caps. Such an application could also make it possible to assess a potential added value of a wind shear-dependent formulation of the mixing length. Moreover, in view of a fully reliable application in a climate model such as LMDZ, the key parameters of the ATKE scheme - especially c_l and c_ϵ - should be included in a more thorough tuning exercise including parameters from other parameterizations and considering additional metrics on convective boundary layer simulations (Hourdin et al., 2021).

Last but not least, we would like to emphasize that this work was initiated and fostered during collaborative work sessions dedicated to the transfer of knowledge and critical questioning on the physics and assumptions behind the parameterizations used in planetary GCMs. Those sessions spontaneously emerged following students' questions and gathered atmospheric and planetary scientists experts and non experts of turbulent mixing and parameterization development. The motivations behind the ATKE scheme development went beyond the need to advance the turbulent diffusion scheme in our models but were also - and maybe firstly - a reason and a need to teach and learn the parameterization development in a 'learning-by-doing' way.

Appendix A A gravity-invariant formulation of our TKE-l turbulent diffusion scheme

For the sake of universality of a turbulent diffusion parameterization and in particular for potential application on different planets, one may want to develop a framework as independent as possible upon planet's characteristics, in particular upon planet's gravity. In the main paper, gravity appears in the expression of the Brünt Väisälä frequency thus in the expression of the gradient Richardson number and in the buoyancy term of the TKE evolution equation Eq 7. In this appendix, we briefly introduce a framework using geopotential as vertical coordinate and in which gravity is no longer involved. Such a framework is proposed here as a prospect for a further new implementation of the parameterisation.

Let's introduce the geopotential ϕ defined such that $d\phi = gdz$ as well as a 're-scaled' time τ defined by $d\tau = gdt$ The diffusion equation of a quantity c (Eq. 5) can be written in the form:

$$\frac{\partial c}{\partial \tau} = \frac{1}{\rho} \frac{\partial}{\partial \phi} \left(\rho K_c^\phi \frac{\partial c}{\partial \phi} \right) \tag{A1}$$

where $K_c^\phi = gK_c$. In such a framework, assuming down-gradient expression of turbulent fluxes and the same closures for the TKE dissipation and transport terms as in the main manuscript, the TKE evolution equation A1 reads:

$$\frac{\partial e}{\partial \tau} = K_m^\phi \left[(S^\phi)^2 - Pr(Ri)(N^\phi)^2 \right] + \frac{1}{\rho} \frac{\partial}{\partial \phi} (\rho c_e K_m^\phi \frac{\partial e}{\partial \phi}) - \frac{e^{3/2}}{c_\epsilon l^\phi} \tag{A2}$$

with $l^\phi = gl$, $(S^\phi)^2 = (\partial_\phi u)^2 + (\partial_\phi v)^2$ and $(N^\phi)^2 = \frac{1}{\theta_v} \frac{\partial \theta_v}{\partial \phi}$.

One can then express $K_m^\phi = l^\phi(\phi, e, Ri) S_m(Ri) \sqrt{e}$. Noting the gravity independent form of the gradient Richardson number $Ri = (N^\phi)^2/(S^\phi)^2$, the expressions for $S_m(Ri)$ and $Pr(Ri)$ can be taken identically from Eq. 20 and 23 as they are gravity-independent. For the mixing length l^ϕ expression, one can use a similar approach as in Sect. 2.4 replacing the neutral-limit formulation with

$$l_n^\phi = \frac{\kappa \phi l_\infty^\phi}{\kappa \phi + l_\infty^\phi} \tag{A3}$$

l_∞^ϕ being a tuning parameter. In such a way Eq. A1 and A2 combined with the proposed expressions for K_m, Pr and l^ϕ establish a complete gravity-invariant formulation of the turbulent diffusion parameterization.

Open Research Section

The latest version of the LMDZ source code can be downloaded freely from the LMDZ web site. The version used for the specific simulation runs for this paper is the 'svn' release 4781 from 21 December 2023, which can be downloaded and installed on a Linux

computer by running the install_lmdz.sh script available here: `http://www.lmd.jussieu.fr/\tilde/pub/install_lmdz.sh`. The Mars PCM used in this work can be downloaded with documentation from the SVN repository at `https://svn.lmd.jussieu.fr/Planeto/trunk/LMDZ.MARS/`. Forcings for the GABLS1 single-column cases are provided under the DEPHY-SCM standard at the following link: `https://github.com/GdR-DEPHY/DEPHY-SCM/`. GABLS1 LES used in the intercomparison exercise of Beare et al. (2006) are distributed here: `https://gabls.metoffice.gov.uk/lem_data.html`
Dome C temperature and wind speed data are freely distributed on PANGAEA data repositories at `https://doi.org/10.1594/PANGAEA.932512` and `https://doi.org/10.1594/PANGAEA.932513`. InSight wind data can be retrieved from the Planetary Data System (Jose Rodriguez-Manfredi, 2019).

Acknowledgments

This project has received funding from the European Research Council (ERC) under the European Union's Horizon 2020 research and innovation programme (grant no. 951596) through the AWACA project. The part of the work related to the Martian atmosphere is supported by the ANR project MAGIS. We acknowledge support from the DEPHY research group, funded by CNRS/INSU and Météo-France, as well as from the PEPR TRACCS project (no. ANR-22-EXTR-0008) funded from the Agence Nationale de la Recherche - France 2030. Éric Bazile is gratefully acknowledged for fruitful discussions. This study was conducted using the ESPRI (Ensemble de Services Pour la Recherche l'IPSL) computing and data center (https://mesocentre.ipsl.fr) which is supported by CNRS, Sorbonne Université, Ecole Polytechnique, and CNES and through national and international grants. Simulations were performed using HPC resources from the IDRIS (Institut du Développement et des Ressources en Informatique Scientifique, CNRS, France), project RLMD AD010107632R1. Simulations with the Mars PCM were performed using HPC resources of Centre Informatique National de l'Enseignement Supérieur (CINES) under the allocation n°A0100110391 made by Grand Equipement National de Calcul Intensif (GENCI).

References

Acevedo, O. C., Mahrt, L., Puhales, F. S., Costa, F. D., Medeiros, L. E., & Degrazia, G. A. (2015). Contrasting structures between the decoupled and coupled states of the stable boundary layer. *Q J R Meteorol Soc*, *142*(695), 693-702. (doi: 10.1002/qj.2693)

André, J. C., Moor, G. D., Lacarrère, P., & du Vachat, R. (1978). Modeling the 24-hour evolution of the mean and turbulent structures of the planetary boundary layer. *Journal of Atmospheric Sciences*, *35*(10), 1861 - 1883. Retrieved from `https://journals.ametsoc.org/view/journals/atsc/35/10/1520-0469_1978_035_1861_mtheot_2_0_co_2.xml` doi: https://doi.org/10.1175/1520-0469(1978)035⟨1861:MTHEOT⟩2.0.CO;2

Audouin, O., Roehrig, R., Couvreux, F., & Williamson, D. (2021). Modeling the gabls4 strongly-stable boundary layer with a gcm turbulence parameterization: Parametric sensitivity or intrinsic limits? *Journal of Advances in Modeling Earth Systems*, *13*(3), e2020MS002269. doi: https://doi.org/10.1029/2020MS002269

Baas, P., Van De Wiel, B., Van der Linden, S., & Bosveld, F. (2018). From near-neutral to strongly stratified: Adequately modelling the clear-sky nocturnal boundary layer at cabauw. *Boundary-Layer Meteorology*, *166*, 217–238.

Baas, P., van de Wiel, B. J. H., van Meijgaard, E., Vignon, E., Genthon, C., van der Linden, S. J. A., & de Roode, S. R. (2019). Transitions in the wintertime near-surface temperature inversion at dome c, antarctica. *Quarterly Journal of the Royal Meteorological Society*, *145*(720), 930-946. doi: https://doi.org/10.1002/qj.3450

Banfield, D., Spiga, A., Newman, C., Forget, F., Lemmon, M., Lorenz, R., ... others (2020). The atmosphere of mars as observed by insight. *Nature Geoscience*, *13*(3), 190–198.

Bazile, E., Marquet, P., Bouteloup, Y., & Bouyssel, F. (2011). The turbulent kinetic energy (tke) scheme in the nwp models at météo-france. In *Workshop on diurnal cycles and the stable boundary layer, ecmwf* (pp. 127–136).

Beare, R. J., Macvean, M. K., Holtslag, A. A. M., Cuxart, J., Esau, I., Golaz, J.-C., ... Sullivan, P. (2006). An intercomparison of large-eddy simulations of the stable boundary layer. *Boundary-Layer Meteorology*, *118*(2), 247–272. doi: 10.1007/s10546-004-2820-6

Betts, A. K. (1973). Non-precipitating cumulus convection and its parameterization. *Quarterly Journal of the Royal Meteorological Society*, *99*(419), 178-196. Retrieved from `https://rmets.onlinelibrary.wiley.com/doi/abs/10.1002/qj.49709941915` doi: https://doi.org/10.1002/qj.49709941915

Blackadar, A. K. (1962). The vertical distribution of wind and turbulent exchange in neutral atmosphere. *J Geophys Res*, *67*, 3095-3102.

Boucher, O., Servonnat, J., Albright, A. L., Aumont, O., Balkanski, Y., Bastrikov, V., ... Vuichard, N. (2020). Presentation and evaluation of the ipsl-cm6a-lr climate model. *Journal of Advances in Modeling Earth Systems*, *12*(7), e2019MS002010. doi: 10.1029/2019MS002010

Bougeault, P., & Lacarrère, P. (1989). Parametrization of orography-induced turbulence in a mesobeta-scale model. *Monthly-Weather Rev*, *117*, 1872-1891.

Chatain, A., Spiga, A., Banfield, D., Forget, F., & Murdoch, N. (2021). Seasonal variability of the daytime and nighttime atmospheric turbulence experienced by insight on mars. *Geophysical Research Letters*, *48*(22), e2021GL095453. Retrieved from `https://agupubs.onlinelibrary.wiley.com/doi/abs/10.1029/2021GL095453` doi: https://doi.org/10.1029/2021GL095453

Chen, W., Lovejoy, S., & Muller, J.-P. (2016). Mars' atmosphere: The sister planet, our statistical twin. *Journal of Geophysical Research: Atmospheres*, *121*(20), 11,968-11,988. doi: https://doi.org/10.1002/2016JD025211

Cheruy, F., Ducharne, A., Hourdin, F., Musat, I., Vignon, , Gastineau, G., ... Zhao, Y. (2020). Improved near-surface continental climate in ipsl-cm6a-lr by combined evolutions of atmospheric and land surface physics. *Journal of Advances in Modeling Earth Systems*, *12*(10), e2019MS002005. doi: https://doi.org/10.1029/2019MS002005

Colaïtis, A., Spiga, A., Hourdin, F., Rio, C., Forget, F., & Millour, E. (2013). A thermal plume model for the Martian convective boundary layer. *Journal of Geophysical Research: Planets*, *118*(7), 1468-1487. doi: 10.1002/jgre.20104

Couvreux, F., Bazile, E., Rodier, Q., Maronga, B., Matheou, G., Chinita, M. J., ... others (2020). Intercomparison of large-eddy simulations of the antarctic boundary layer for very stable stratification. *Boundary-Layer Meteorology*, *176*(3), 369–400. doi: 10.1007/s10546-020-00539-4

Couvreux, F., Hourdin, F., Williamson, D., Roehrig, R., Volodina, V., Villefranque, N., ... Xu, W. (2021). Process-based climate model development harnessing machine learning: I. a calibration tool for parameterization improvement. *Journal of Advances in Modeling Earth Systems*, *13*(3), e2020MS002217. Retrieved from `https://agupubs.onlinelibrary.wiley.com/doi/abs/10.1029/2020MS002217` doi: https://doi.org/10.1029/2020MS002217

Cuxart, J., Holtslag, A. A. M., Beare, R. J., Bazile, E., Beljaars, A., Cheng, A., ... Xu, K.-M. (2006). Single-column model intercomparison for a stably stratified atmospheric boundary layer. *Boundary-Layer Meteorol*, *118*(2), 273-303. (doi:10.1007/s10546-005-3780-1)

Deardoff, J. W. (1980). Stratocumulus-capped mixed layers derived from a threee dimensionnal model. *Boundary-Layer Meteorol*, *18*, 495-527.

Delage, Y. (1997). Parametrising sub-grid scale vertical transport in atmospheric models under statically stable conditions. *Boundary-Layer Meteorol*, *82*, 23-48.

Deleersnijder, E. (1992). *Modélisation hydrodynamique tridimensionnelle de la circulation générale estivale de la région du détroit de bering (in french)* (Unpublished doctoral dissertation). Université Catholique de Louvain.

Derbyshire, S. H. (1990). Nieuwstadt's stable boundary layer revisited. *Q J R Meteorol*

Soc, *126*, 127-158.
Dufresne, J.-L., & Ghattas, J. (2009). Description du schéma de la couche limite turbulente et l'interface avec la surface planetaire dans lmdz. *ORCHIDEE documentation*. Retrieved from http://forge.ipsl.jussieu.fr/orchidee/attachment/wiki/Documentation/CouplingLMDZ/Dufresne,\%20Ghattas\%20-\%202009_Coupling-ORC-LMDZ.pdf (in french)
Edwards, J. M. (2009). Radiative processes in the stable boundary layer: Part i. radiatives aspects. *Boundary-Layer Meteorology*, *131*(1). doi: 10.1007/s10546-009-9364-8
Emanuel, K. A. (1991). A scheme for representing cumulus convection in large-scale models. *Journal of Atmospheric Sciences*, *48*(21), 2313 - 2329. doi: https://doi.org/10.1175/1520-0469(1991)048⟨2313:ASFRCC⟩2.0.CO;2
England, D. E., & McNider, R. T. (1995). Stability functions based upon shear functions. *Boundary-Layer Meteorol*, *74*, 113-130.
Forget, F., Banfield, D., Spiga, A., Millour, E., Borella, A., Lange, L., ... Banerdt, W. B. (2021). More than one Martian year of meteorology observed by the InSight Lander. In *European planetary science congress* (p. EPSC2021-273). doi: 10.5194/epsc2021-273
Forget, F., Hourdin, F., Fournier, R., Hourdin, C., Talagrand, O., Collins, M., ... Huot, J.-P. (1999). Improved general circulation models of the martian atmosphere from the surface to above 80 km. *Journal of Geophysical Research: Planets*, *104*(E10), 24155-24175. Retrieved from https://agupubs.onlinelibrary.wiley.com/doi/abs/10.1029/1999JE001025 doi: https://doi.org/10.1029/1999JE001025
Genthon, C., Veron, D., Vignon, E., Six, D., Dufresne, J.-L., Madeleine, J.-B., ... Forget, F. (2021). 10 years of temperature and wind observation on a 45 m tower at dome c, east antarctic plateau. *Earth System Science Data*, *13*(12), 5731–5746. Retrieved from https://essd.copernicus.org/articles/13/5731/2021/ doi: 10.5194/essd-13-5731-2021
Girard, C., & Delage, Y. (1990). Stable schemes for nonlinear vertical diffusion in atmospheric circulation models. *Monthly Weather Review*, *118*(3), 737 - 745. Retrieved from https://journals.ametsoc.org/view/journals/mwre/118/3/1520-0493_1990_118_0737_ssfnvd_2_0_co_2.xml doi: https://doi.org/10.1175/1520-0493(1990)118⟨0737:SSFNVD⟩2.0.CO;2
Golaz, J.-C., Larson, V. E., & Cotton, W. R. (2002). A pdf-based model for boundary layer clouds. part i: Method and model description. *Journal of the Atmospheric Sciences*, *59*(24), 3540 - 3551. Retrieved from https://journals.ametsoc.org/view/journals/atsc/59/24/1520-0469_2002_059_3540_apbmfb_2.0.co_2.xml doi: https://doi.org/10.1175/1520-0469(2002)059⟨3540:APBMFB⟩2.0.CO;2
Grisogono, B. (2010). Generalizing 'z-less' mixing length for stable boundary layers. *Quarterly Journal of the Royal Meteorological Society*, *136*(646), 213-221. doi: https://doi.org/10.1002/qj.529
Grisogono, B., & Belušić, D. (2008). Improving mixing length-scale for stable boundary layers. *Quarterly Journal of the Royal Meteorological Society*, *134*(637), 2185-2192. Retrieved from https://rmets.onlinelibrary.wiley.com/doi/abs/10.1002/qj.347 doi: https://doi.org/10.1002/qj.347
He, Y., McFarlane, N. A., & Monahan, A. H. (2019). A new tke-based parameterization of atmospheric turbulence in the canadian global and regional climate models. *Journal of Advances in Modeling Earth Systems*, *11*(5), 1153-1188. doi: https://doi.org/10.1029/2018MS001532
Hersbach, H., Bell, B., Berrisford, P., Hirahara, S., Horányi, A., Muñoz-Sabater, J., ... Thépaut, J.-N. (2020). The era5 global reanalysis. *Quarterly Journal of the Royal Meteorological Society*, *146*, 1999-2049. doi: 10.1002/qj.3803
Holtslag, A. A. M., & Boville, B. A. (1993). Local versus non-local boundary layer diffusion in a global climate model. *J Clim*, *6*, 1825-1842.
Holtslag, A. A. M., Svensson, G., Baas, P., Basu, S., Beare, B., Beljaars, A. C. M., ... Van de Wiel, B. J. H. (2013). Stable boundary layers and diurnal cycles. *Bull Amer Meteor Soc*, *94*, 1691-1706. (doi:10.1175/BAMS-D-11-00187.1.)

Hourdin, F., Couvreaux, F., & Menut, L. (2002). Parameterization of the dry convective boundary layer based on a mass flux representation of thermals. *J Atmos Sci*, *59*, 1105-1123.

Hourdin, F., Jam, A., Rio, C., Couvreux, F., Sandu, I., Lefebvre, M.-P., ... Idelkadi, A. (2019). Unified parameterization of convective boundary layer transport and clouds with the thermal plume model. *Journal of Advances in Modeling Earth Systems*, *11*(9), 2910-2933. doi: https://doi.org/10.1029/2019MS001666

Hourdin, F., Rio, C., Grandpeix, J.-Y., Madeleine, J.-B., Cheruy, F., Rochetin, N., ... Ghattas, J. (2020). Lmdz6a: the atmospheric component of the ipsl climate model with improved and better tuned physics. *Journal of Advances in Modeling Earth Systems*. doi: 10.1029/2019MS001892

Hourdin, F., Williamson, D., Rio, C., Couvreux, F., Roehrig, R., Villefranque, N., ... Volodina, V. (2021). Process-based climate model development harnessing machine learning: Ii. model calibration from single column to global. *Journal of Advances in Modeling Earth Systems*, *13*(6), e2020MS002225. Retrieved from `https://agupubs.onlinelibrary.wiley.com/doi/abs/10.1029/2020MS002225` doi: https://doi.org/10.1029/2020MS002225

Jose Rodriguez-Manfredi. (2019). *Apss twins data.* NASA Planetary Data System. Retrieved from `https://pds.nasa.gov/ds-view/pds/viewBundle.jsp?identifier=urn:nasa:pds:insight_twins&version=3.2` doi: 10.17189/1518950

Kahre, M. A., Murphy, J. R., Newman, C. E., Wilson, R. J., Cantor, B. A., Lemmon, M. T., & Wolff, M. J. (2017). The Mars dust cycle. In *The atmosphere and climate of Mars* (p. 295–337). Cambridge University Press. doi: 10.1017/9781139060172.010

Kalnay, E., & Kanamitsu, M. (1988). Time schemes for strongly nonlinear damping equations. *Monthly Weather Review*, *116*(10), 1945 - 1958. Retrieved from `https://journals.ametsoc.org/view/journals/mwre/116/10/1520-0493_1988_116_1945_tsfsnd_2_0_co_2.xml` doi: https://doi.org/10.1175/1520-0493(1988)116⟨1945:TSFSND⟩2.0.CO;2

Kolmogorov, A. N. (1941). Energy dissipation in locally isotropic turbulence. *Doklady AN SSSR*, *32*, 19-21.

Lange, L., Forget, F., Dupont, E., Vandemeulebrouck, R., Spiga, A., Millour, E., ... Bierjon, A. (2023). Modeling slope microclimates in the mars planetary climate model. *Journal of Geophysical Research: Planets*, *128*(10), e2023JE007915. doi: 10.1029/2023JE007915

Lenderink, G., & Holtslag, A. A. M. (2000). Evaluation of the kinetic energy approach for modeling turbulent fluxesin stratocumulus. *Monthly Weather Review*, *128*(1), 244 - 258. Retrieved from `https://journals.ametsoc.org/view/journals/mwre/128/1/1520-0493_2000_128_0244_eotkea_2.0.co_2.xml` doi: https://doi.org/10.1175/1520-0493(2000)128⟨0244:EOTKEA⟩2.0.CO;2

Lenderink, G., & Holtslag, A. A. M. (2004). An updated length-scale formulation for turbulent mixing in clear and cloudy boundary layers. *Quarterly Journal of the Royal Meteorological Society*, *130*(604), 3405-3427. Retrieved from `https://rmets.onlinelibrary.wiley.com/doi/abs/10.1256/qj.03.117` doi: https://doi.org/10.1256/qj.03.117

Li, D. (2019). Turbulent prandtl number in the atmospheric boundary layer - where are we now? *Atmospheric Research*, *216*, 86-105. Retrieved from `https://www.sciencedirect.com/science/article/pii/S0169809518307324` doi: https://doi.org/10.1016/j.atmosres.2018.09.015

Li, D., Katul, G. G., & Zilitinkevich, S. S. (2016). Closure schemes for stably stratified atmospheric flows without turbulence cutoff. *Journal of the Atmospheric Sciences*, *73*(12), 4817 - 4832. doi: https://doi.org/10.1175/JAS-D-16-0101.1

Louis, J.-F. (1979). A parametric model of vertical eddy fluxes in the atmosphere. *Boundary-Layer Meteorol*, *17*, 187-202. (doi: 10.1007/BF00712379)

Louis, J. F., Tiedtke, M., & Geleyn, J.-F. (1982). A short history of the operational pbl parametrization at ECMWF. *Paper presented at the ECMWF workshop on boundary*

layer parametrization, ECMWF, Reading.
Mašek, J., Ďurán, I. B., & Brožková, R. (2022). Stable numerical implementation of a turbulence scheme with two prognostic turbulence energies. *Monthly Weather Review*, *150*(7), 1667 - 1688. Retrieved from `https://journals.ametsoc.org/view/journals/mwre/150/7/MWR-D-21-0172.1.xml` doi: https://doi.org/10.1175/MWR-D-21-0172.1
Mellor, G. L., & Yamada, T. (1974). A hierarchy of turbulence closure models for planetary boundary layers. *J Atmos Sci*, *30*, 1061-1069.
Mellor, G. L., & Yamada, T. (1982). Development of a turbulence closure model for geophysical fluid problems. *Rev Geophys Space Phys*, *20*(4), 851-875.
Montabone, L., Forget, F., Millour, E., Wilson, R., Lewis, S., Cantor, B., ... Wolff, M. (2015). Eight-year climatology of dust optical depth on mars. *Icarus*, *251*, 65–95. doi: 10.1016/j.icarus.2014.12.034
Nieuwtsadt, F. T. M. (1984). The turbulent structure of the stable, nocturnal boundary layer. *J Atmos Sci*, *41*, 2202-2217.
Petrosyan, A., Galperin, B., Larsen, S. E., Lewis, S. R., Määttänen, A., Read, P. L., ... Vázquez, L. (2011). The martian atmospheric boundary layer. *Reviews of Geophysics*, *49*(3). Retrieved from `https://agupubs.onlinelibrary.wiley.com/doi/abs/10.1029/2010RG000351` doi: https://doi.org/10.1029/2010RG000351
Pottier, A., Forget, F., Montmessin, F., Navarro, T., Spiga, A., Millour, E., ... Madeleine, J.-B. (2017). Unraveling the martian water cycle with high-resolution global climate simulations. *Icarus*, *291*, 82–106. doi: 10.1016/j.icarus.2017.02.016
Rio, C., Hourdin, F., Couvreux, F., & Jam, A. (2010). Resolved versus parametrized boundary-layer plumes. Part II: continuous formulations of mixing rates for mass-flux schemes. *Boundary-layer Meteorol*. (Doi:10.1007/s10546-010-9478)
Rodier, Q., Masson, V., Couvreux, F., & Paci, A. (2017). Evaluation of a buoyancy and shear based mixing length for a turbulence scheme. *Frontiers in Earth Science*, *5*, 65. doi: 10.3389/feart.2017.00065
Sandu, I., Beljaars, A., Bechtold, P., Mauritsen, T., & Balsamo, G. (2013). Why is it so difficult to represent stably stratified conditions in numerical weather prediction (nwp) models. *J Adv Model Earth Syst*, *5*, 117-133. (doi: 10.1002/jame.20013)
Spiga, A., Forget, F., Lewis, S. R., & Hinson, D. P. (2010a). Structure and dynamics of the convective boundary layer on mars as inferred from large-eddy simulations and remote-sensing measurements. *Quarterly Journal of the Royal Meteorological Society*, *136*(647), 414-428. Retrieved from `https://rmets.onlinelibrary.wiley.com/doi/abs/10.1002/qj.563` doi: https://doi.org/10.1002/qj.563
Spiga, A., Forget, F., Lewis, S. R., & Hinson, D. P. (2010b). Structure and dynamics of the convective boundary layer on Mars as inferred from large-eddy simulations and remote-sensing measurements. *Quarterly Journal of the Royal Meteorological Society*, *136*(647), 414-428. doi: 10.1002/qj.563
Stull, R. B. (1990). *An introduction to boundary layer meteorology.* Kluver, Boston.
Sun, J. (2011). Vertical variations of mixing lengths under neutral and stable conditions during cases-99. *Journal of Applied Meteorology and Climatology*, *50*(10), 2030 - 2041. Retrieved from `https://journals.ametsoc.org/view/journals/apme/50/10/jamc-d-10-05006.1.xml` doi: https://doi.org/10.1175/JAMC-D-10-05006.1
Tiedtke, M. (1989). A comprehensive mass flux scheme for cumulus parameterization in large-scale models. *Monthly Weather Review*, *117*(8), 1779 - 1800. doi: https://doi.org/10.1175/1520-0493(1989)117⟨1779:ACMFSF⟩2.0.CO;2
van der Linden, S. J., Edwards, J. M., van Heerwaarden, C. C., Vignon, E., Genthon, C., Petenko, I., ... van de Wiel, B. J. (2019). Large-eddy simulations of the steady wintertime antarctic boundary layer. *Boundary-Layer Meteorology*, *173*(2), 165–192. doi: 10.1007/s10546-019-00461-4
van de Wiel, B. J. H., Moene, A. F., H., D. R. W., & Jonker, H. J. J. (2008). Local similarity in the stable boundary layer and mixing-length approaches: consistency of concepts. *Boundary-Layer Metorol*, *128*, 103-116.

van de Wiel, B. J. H., Moene, A. F., Steeneveld, G. J., Baas, P., Bosveld, F. C., & Holstlag, A. A. M. (2010). A conceptual view on inertial oscillations and nocturnal low-level jets. *J Atmos Sci*, *67*, 2679-2689. (doi: 10.1175/2010JAS3289.1)

van de Wiel, B. J. H., Vignon, E., Baas, P., van Hooijdonk, I. G. S., van der Linden, S. J. A., van Hooft, J. A., ... Genthon, C. (2017). Regime transition in near-surface temperature inversions: a conceptual model. *J Atmos Sci*, *74*, 1057-1073. (doi:10.1175/JAS-D-16-0180.1)

Venayagamoorthy, S. K., & Stretch, D. D. (2010). On the turbulent prandtl number in homogeneous stably stratified turbulence. *Journal of Fluid Mechanics*, *644*, 359–369. doi: 10.1017/S002211200999293X

Vignon, E., Hourdin, F., Genthon, C., Gallée, H., Bazile, E., Lefebvre, M.-P., ... Van de Wiel, B. J. H. (2017). Parametrization of the boundary layer over the antarctic plateau in a general circulation model: 1D simulations against summertime observations at Dome C. *J Geophys Res Atmos*, *122*. (doi: 10.1002/2017JD026802)

Vignon, E., Hourdin, F., Genthon, C., Van de Wiel, B. J. H., , Gallée, H., ... Beaumet, J. (2018). Modeling the dynamics of the atmospheric boundary layer over the antarctic plateau with a general circulation model. *Journal of Advances in Modeling Earth Systems*. (10.1002/2017MS001184)

Vignon, E., van de Wiel, B. J. H., van Hooijdonk, I. G. S., Genthon, C., van der Linden, S. J. A., van Hooft, J. A., ... Casasanta, G. (2017). Stable boundary layer regimes at Dome C, Antarctica: observation and analysis. *Q J R Meteorol Soc*, *143*(704), 1241-1253. (doi:10.1002/qj.2998)

Weiss, B. P., & Ingersoll, A. P. (2000). Cold spots in the martian polar regions: Evidence of carbon dioxide depletion? *Icarus*, *144*(2), 432-435. doi: 10.1006/icar.1999.6302

Yamada, T. (1975). A simulation of the wangara atmospheric boundary layer data. *J Atmos Sci*, *32*, 2309-2320.

Yamada, T. (1983). Simulations of nocturnal drainage flows by a q^2l turbulence closure model. *J Atmos Sci*, *40*, 91-106.

Zilitinkevich, S., Elperin, T., Kleeorin, N., & Rogachevskii, I. (2007). Energy and flux-budget turbulence closure model for stably stratified flows. Part I: Steady state, homogeneous regime. *Boundary-Layer Meteorol*, *125*, 167-191. (doi:10.1007/s10546-007-9189-2)

Zilitinkevich, S., Elperin, T., Kleeorin, N., Rogachevskii, I., Esau, I., Mauritsen, T., & Miles, M. W. (2008). Turbulence energetics in stably stratified geophysical flows: Strong and weak mixing regimes. *Q J R Meteorol Soc*, *134*, 793-799. (doi:10.1002/qj.264)